

1 **Slide-hold-slide protocols and frictional healing in a simulated**
2 **granular fault gouge**

3 **Behrooz Ferdowsi¹, Allan M. Rubin¹**

4 ¹Department of Geosciences, Princeton University, Princeton, NJ 08544, USA

5 **Key Points:**

- 6 • We examined the behavior of a simulated sheared granular layer with time-independent
7 contact-scale properties in slide-hold-slide protocols.
8 • The slide-hold simulations with different model stiffnesses mimic the stress decay response
9 of laboratory friction data.
10 • As with lab data, the peak stress upon resliding increases linearly with log hold time, with a
11 slope close to the rate-state 'b'.

Abstract

The empirical constitutive modeling framework of Rate- and State-dependent Friction (RSF) is commonly used to describe the time-dependent frictional response of fault gouge to perturbations from steady sliding. In a previous study (Ferdowsi & Rubin, 2020), we found that a granular-physics-based model of a fault shear zone, with time-independent properties at the contact scale, reproduces the phenomenology of laboratory rock and gouge friction experiments in velocity-step and slide-hold protocols. A few slide-hold-slide simulations further suggested that the granular model might outperform current empirical RSF laws in describing laboratory data. Here, we explore the behavior of the same model in slide-hold and slide-hold-slide protocols over a wide range of sliding velocities, hold durations, and system stiffnesses, and provide additional support for this view. We find that, similar to laboratory data, the rate of stress decay during slide-hold simulations is in general agreement with the “Slip law” version of the RSF equations, using parameter values determined independently from velocity step tests. During reslides following long hold times, the model, similar to lab data, produces a nearly constant rate of frictional healing with log hold time, with that rate being in the range of $\sim 0.5 - 1$ times the RSF “state evolution” parameter b . We also find that, as in laboratory experiments, the granular layer undergoes log-time compaction during holds. This is consistent with the traditional understanding of state evolution under the Aging law, even though the associated stress decay is similar to that predicted by the Slip and not the Aging law.

1 Introduction

The constitutive framework of Rate- and State-dependent Friction is often used for modeling transient frictional behavior of rocks and other Earth materials (e.g., sediment, glacial till), and for simulating frictional instabilities relevant to earthquakes, landslides and earthflows (J. H. Dieterich, 1992, 1978, 1979; J. H. Dieterich et al., 1981; Ruina, 1983; J. Dieterich, 1994; Marone, 1998; J. H. Dieterich & Kilgore, 1996; Viesca, 2016; Handwerker et al., 2016; McCarthy et al., 2017). A complete prescription of RSF requires an equation for the evolution of the “state variable” defining the “state” of the sliding interface. Existing versions of this equation are largely empirical, differ fundamentally in the extent to which slip or elapsed time is responsible for state evolution, and fail to satisfactorily match the suite of laboratory experiments they were designed to describe.

A popular concept has been that in the absence of sliding, state evolution (frictional strengthening, in such cases) is fundamentally a time-dependent process (J. H. Dieterich, 1972). This hypothesis has received support first from the observed logarithmic-with-time growth of contact area between transparent samples of PMMA (Polymethyl methacrylate), due to plastic deformation of contacting asperities (J. H. Dieterich & Kilgore, 1994), and more recently from the logarithmic-with-time increase in acoustic transmissivity across frictional interfaces in rock (Nagata et al., 2012). Log-time frictional strengthening of stationary surfaces has been shown to also result from increased chemical bonding (Li et al., 2011). The log-time increase in both contact area and chemical bonding have been shown to have a sound theoretical basis (Berthoud et al., 1999; Baumberger & Caroli, 2006; Liu & Szlufarska, 2012). Such behavior is embodied in the “Aging” (or “Dieterich”) equation for state evolution (Ruina, 1983). Despite its theoretical basis, however, the Aging law accurately describes almost no rock or gouge friction data other than the observed increase in “static” friction with the logarithm of hold time in laboratory slide-hold-slide experiments (as measured by the friction peak upon resliding).

In contrast, a second popular equation for state evolution (the “Slip” or “Ruina” law) has no well-established theoretical justification, but does a remarkably good job describing the results of laboratory velocity-step experiments, as well as the stress decay during the hold portion of slide-hold-slide experiments (Ruina, 1983; Nakatani, 2001; Bhattacharya et al., 2015, 2017). The Aging and Slip laws are asymptotically identical for small perturbations from steady-state sliding, but diverge as the sliding deviates further from steady state. Notably, unlike the Aging law, the Slip law predicts no state evolution in the absence of slip. Nonetheless, the Slip law can still generate an increase in frictional strength approximately as log hold time during slide-hold-slide experiments,

63 due to the small amount of slip accompanying the stress decay during holds applied by an elastic
64 testing machine (Ruina, 1983).

65 The lack of a physics-based theory for transient friction of rock has motivated exploring the
66 physical and chemical origins of rate-state friction in a variety of scientific communities, and has
67 also brought significant attention to the contributions of the quantity (contact area) versus the quality
68 (shear strength) of contact asperities to the state of a frictional interface (Li et al., 2011; Chen
69 & Spiers, 2016; Tian et al., 2017, 2018; Thom et al., 2018). However, future investigations are
70 needed to address the implications of asperity-scale (sometimes single-asperity-scale) observations
71 for the transient frictional behavior at the macroscopic scale. In addition, more work is necessary
72 to determine if any of the single-asperity-scale observations may reproduce or explain the transient
73 frictional behavior of rock and gouge materials in the lab.

74 In a previous study, we used the discrete element method to simulate the transient frictional
75 behavior of a sheared granular gouge layer in a loading configuration that mimicked traditional rock
76 friction experiments (Ferdowsi & Rubin, 2020). We intentionally implemented constant Coulomb
77 friction and no time-dependence of the properties at grain-grain contacts. We then subjected this
78 simulated fault gouge to a series of velocity-stepping protocols. It is noteworthy that most labo-
79 ratory rock friction experiments become to some extent granular gouge experiments after a short
80 shearing displacement, as a result of wear products that develop on even initially bare rock sliding
81 surfaces, and that the RSF phenomenology is observed in both those experiments that start with
82 bare rock surfaces and those that start with a synthetic gouge layer (Marone, 1998). We found
83 that the sheared granular model, like the Slip law for state evolution, successfully reproduces the
84 characteristic transient frictional response of rock and gouge observed in laboratory velocity-step
85 tests. Furthermore, in that study we investigated a limited number of slide-hold and slide-hold-slide
86 (SHS) tests, and found that the stress decay during the holds were consistent with the predictions
87 of the Slip law, which itself is largely consistent with the stress decay observed in laboratory slide-
88 hold experiments. During the reslides, on the other hand, the simulations deviated from the Slip
89 law prediction, and it did so in a manner that seemed more consistent with laboratory experiments.
90 Together, these results suggested that the granular flow model might do a better job of describing
91 (room temperature, nominally dry) rock and gouge friction experiments than the existing, largely
92 empirical RSF equations. This is surprising. By eliminating time-dependent chemical reactions and
93 plasticity at grain/grain contacts, we are dispensing with what is traditionally considered to be the
94 source of the rate- and state-dependence of rock friction. All the velocity-dependence and transient
95 response of the granular flow model results from momentum transfer between grains, even at our
96 lowest imposed sliding velocities of 10^{-4} m/s.

97 The purpose of the present paper is to further test the granular flow model as a descriptor of
98 rock friction by more thoroughly examining SHS protocols. Most importantly, for comparison to
99 lab data, we explore a wider range of system stiffnesses. All the SHS simulations in Ferdowsi and
100 Rubin (2020) were conducted at the highest stiffness we could achieve, that limit being set by the
101 elastic stiffness of the gouge layer itself. For velocity-step tests this is desirable; a high stiffness
102 ensures that the inelastic sliding velocity is always nearly the load point velocity, which allows
103 one to infer the RSF parameters directly from the transient frictional response without having to
104 account for a varying velocity. However, for slide-hold tests the inelastic velocity during the hold is
105 always different from the (zero) load-point velocity, and this velocity is controlled to a large extent
106 by the system stiffness. Because the amount of slip during the load-point hold has been used to
107 help distinguish between the roles of slip and time in frictional healing (Beeler et al., 1994), in this
108 paper we use two additional stiffnesses more appropriate for those laboratory experiments. We also
109 employ a wider range of sliding velocities than in Ferdowsi and Rubin (2020), as low as 2 mm/s.
110 This is closer to but still somewhat high by laboratory standards. We return to these points in Section
111 3 of the manuscript.

112 If, in the face of these more stringent SHS tests, the physics-based granular flow model con-
113 tinues to perform well relative to the the empirical RSF equations, it could help further develop our
114 understanding of the processes underlying rate-state friction. In addition, if by interrogating the
115 model output we are also able to understand the physics underlying the transient response of the

116 model to velocity perturbations, it might allow the development of approximate equations that could
 117 be used in numerical simulations of fault slip as a substitute for the RSF equations currently in use.
 118 This provides the motivation, in Section 5, for using the SHS simulations to further explore the possi-
 119 bility that the direct velocity-dependence of friction in the granular simulations can be understood
 120 in terms of the kinetic energy of the gouge particles (Ferdowsi & Rubin, 2020).

121 We note that even if the granular model is successful in this sense, this does not imply that
 122 time-dependent physical and chemical processes at grain contacts are irrelevant. Indeed, numerous
 123 experiments have shown that chemical environment affects the transient behavior of frictional inter-
 124 faces (Frye & Marone, 2002, e.g.). However, at the moment we lack a physical understanding of the
 125 source of RSF (in the sense of also matching most lab friction data) in any system, experimental or
 126 numerical. If we are able to achieve this understanding for the inert granular system, this could shed
 127 light on the origins of similar behavior in quite different systems. For this reason the results of this
 128 study could be of interest to researchers in the fields of granular physics and glassy systems, as well
 129 as, given the ubiquity of granular material in fault zones, researchers in fault mechanics.

130 This paper is organized as follows: In Section 2, we describe the relevant aspects of rate-
 131 state friction, including those aspects that have been seen previously in simulations of granular
 132 flow. Section 3 describes the computational model, and important dimensionless parameters that
 133 can be used to judge how closely our simulations adhere to the laboratory experiments we compare
 134 them to. Section 4 comprises the bulk of the paper - results of the slide-hold and slide-hold-slide
 135 simulations and their comparison to relevant lab experiments and models of RSF. Finally, Section 5
 136 looks at the energetics of the slide-hold simulations, with an eye toward further evaluating the idea
 137 that the granular kinetic energy can be used to understand the source of the instantaneous velocity-
 138 dependence of friction in these simulations.

139 2 Rate- and State-Dependent Friction background

The empirical framework of rate- and state-dependent friction describes the resistance to sliding
 as a function two variables: The sliding rate, V , and “something else”, commonly referred to as the
 “state variable” θ , that describes the “state” of the sliding interface. In its simplest form, RSF
 consists of two equations. The first of these is the “friction equation” alluded to above:

$$\mu = \mu_* + a \log \frac{V}{V_*} + b \log \frac{\theta}{\theta_*}. \quad (1)$$

140 Here μ_* is the nominal steady-state coefficient of friction at the reference velocity V_* and state
 141 θ_* . The RSF parameters a and b control the magnitude of velocity- and state-dependence of the
 142 frictional strength. The second equation is the “state evolution law” describing the time evolution of
 143 the state variable θ . The two commonly used forms are:

$$\text{Aging Law: } \frac{d\theta}{dt} = 1 - \frac{V\theta}{D_c} \quad (2)$$

$$\text{Slip Law: } \frac{d\theta}{dt} = -\frac{V\theta}{D_c} \ln \frac{V\theta}{D_c} \quad (3)$$

144 where D_c is a characteristic slip distance (J. H. Dieterich, 1979; Ruina, 1983). Eq. 2 is often referred
 145 to as the Aging law, as state can evolve with time in the absence of slip; Eq. 3 is often referred to
 146 as the Slip law, as state evolves only with slip ($\dot{\theta} = 0$ when $V = 0$). In general, more than one
 147 state variable might be required to adequately describe friction as observed in the laboratory (Ruina,
 148 1983; Ikari et al., 2016).

149 Previous studies have demonstrated that neither the Aging law nor the Slip law adequately de-
 150 scribes the full range of laboratory velocity-stepping and slide-hold-slide loading protocols (Beeler
 151 et al., 1994; Kato & Tullis, 2001). Velocity-stepping experiments with a sufficiently stiff system

show that following a change in velocity, friction approaches its new steady-state value quasi-exponentially over a characteristic slip distance that is independent of both the magnitude and the sign of the velocity step (Ruina, 1983; Marone, 1998; Blanpied et al., 1998; Bhattacharya et al., 2015). This observation holds for both bare rock and gouge samples, and it is consistent with the Slip law prediction for state evolution because the Slip law was designed with that transient behavior in mind (Ruina, 1983; Nakatani, 2001). However, the Aging law predicts a strongly asymmetric and magnitude-dependent transient frictional response to velocity step increases and decreases, behavior that is completely inconsistent with laboratory data (Nakatani, 2001).

The Aging law was introduced primarily to account for the observation that in SHS experiments, beyond a “cut-off time” that is typically of order 1 s, the peak stress upon resliding increases approximately as the logarithm of the hold time (J. H. Dieterich, 1979; J. H. Dieterich & Kilgore, 1994; Marone & Saffer, 2015; Carpenter et al., 2016). However, Bhattacharya et al. (2017) reanalyzed the experimental SHS data of Beeler et al. (1994), conducted using two different machine stiffnesses (and hence two different amounts of interfacial slip during the load-point hold, as the loading machine and rock sample elastically unload), and found that the log-time increase in peak stress upon resliding could be fit about as well by the Slip law as by the Aging law. Bhattacharya et al. (2017) further showed that the nearly logarithmic-with-time stress decay during the load-point holds could be well modeled by the Slip law, which predicts relatively little state evolution owing to the small amount of slip. In contrast, this log-time stress decay is completely inconsistent with the Aging law, which predicts too much strengthening (state evolution) during the holds, and a rate of stress decay that approaches zero as hold time increases (for $a/b < 1$, as was the case in these experiments). Despite the failure of the Aging law to fit both velocity-step tests and slide-hold tests, most theoretical justifications for the evolution of state presuppose mechanisms of time-dependent healing as embodied by the Aging law (e.g., Baumberger et al., 1999). But even the Slip law is unable to model data from both the hold and reslide portions of SHS tests (Bhattacharya et al., 2017).

2.1 Granular rate- and state-dependent friction

Both the empirical nature and the inadequacies of the existing RSF equations motivated our previous study, in which we modeled the behavior of a granular gouge layer with no time-dependent plasticity or chemistry at the grain contacts (Ferdowsi & Rubin, 2020). We subjected the gouge layer to velocity-step numerical protocols over load-point velocities V_{lp} from 10^{-4} to 2 m/s and normal stresses σ_n from 1 to 25 MPa. We found that, in agreement with RSF and multiple previous DEM modeling studies, the simulated granular layer shows a “direct velocity effect” (i.e., an immediate change in friction of the same sign as the imposed velocity step), that is then followed by a gradual “state evolution effect” as friction evolves in the opposite sense toward its new steady-state value (Morgan, 2004; Hatano, 2009; Abe et al., 2002). We further found that the magnitudes of these frictional transients were proportional to the magnitudes of the logarithm of the velocity change, as in RSF, with values of a and b in equation 1 of ~ 0.02 , not far from values found in the lab.

We also observed that the granular model appeared very similar to lab data during slide-hold tests, in that the stress decay during the hold could be well-modeled by the Slip law for state evolution when using parameter values determined independently from velocity-step tests (Bhattacharya et al., 2017, 2021). The results of our preliminary SHS simulations further indicated that the peak stress upon the reslide exceeds the prediction of the Slip law, using the same parameters that fit the hold well. This is similar to behavior observed in lab data (Bhattacharya et al., 2017). Note that some previous studies also either conceptually or qualitatively showed that frictional healing can occur during SHS tests as a result of compaction within the fault gouge (Sleep, 1995, 1997; Nakatani, 1998; Chen et al., 2020). However, as we noted earlier, the simulations of Ferdowsi and Rubin (2020) employed a stiffness that greatly exceeds those that can be achieved in the laboratory. In the current study we also use stiffnesses more similar to laboratory tests.

200

3 The computational model

201

202

203

204

205

206

207

208

209

210

We have performed the Discrete Element Method (DEM) simulations reported in this study using the *granular* module of LAMMPS (Large scale Atomic/Molecular Massively Parallel Simulator), a multi-scale computational platform developed and maintained by Sandia National Laboratories (<http://lammeps.sandia.gov>) (Plimpton, 1995). Our model is made of a packing of 4815 grains, of which there are 4527 in the gouge layer, and 288 in the top and bottom layers (Figure 1). The grains in those top and bottom layers form rigid blocks parallel to the gouge layer and are used to confine and shear the gouge. The grains in the rigid blocks all have a diameter $d = 5$ mm, whereas those in the gouge layer have a polydisperse, Gaussian-like particle size distribution with diameters (d) from 1 to 5 mm, with a mean diameter (D_{mean}) of 3 mm. Grain density and Young’s modulus are modeled after glass beads (Table S1). The model domain is rectangular with periodic boundary conditions applied in the x and y directions, with domain size $L_x = L_y = 1.5L_z = 20 D_{mean}$.

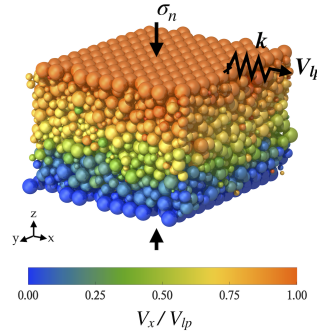


Figure 1. A visualization of the granular gouge simulation. Colors show the velocity of each grain in the x direction, averaged over an upper-plate sliding distance of D_{mean} during steady sliding at a driving velocity of $V_i = 2 \times 10^{-4}$ m/s.

211

212

213

214

215

216

217

218

The system is initially prepared by randomly inserting (under gravity) grains in the simulation box with a desired initial packing fraction of ~ 0.5 . The system is then allowed to relax for about 10^6 time steps, after which it is subjected to confining pressures $\sigma_n = 5$ MPa. The confining pressure is applied for one minute, by which time the fast phase of compaction is completed. The confined gouge sample is then subjected to shearing at a desired driving velocity imposed by a linear spring attached to the top rigid plate, while the vertical position of the top wall is adjusted to maintain a constant confining pressure.

219

220

221

222

223

224

225

226

227

228

229

230

231

232

233

234

We model grains as compressible elastic spheres that interact with each other when they are in contact via the Hertz-Mindlin model (Johnson, 1987; Landau & Lifshitz, 1959; Mindlin, 1949). The full implementation of the granular physics model used here is presented in section 1 of the Supplementary Materials. The model essentially solves the linear vector equation $F = ma$ for each grain, along with its angular counterpart, with the simplification that the model does not track wave propagation through individual grains. In the simulations, slip occurs at grain contacts when the local shear stress exceeds the specified (constant) local friction coefficient. Energy loss at contacts is characterized by the “restitution coefficient”, which potentially varies from 0 (complete energy loss) to 1 (zero loss). The majority of the simulations in this study were performed with a very high restitution coefficient of $\epsilon_n = 0.98$, corresponding roughly to performing experiments on gouge saturated with dry air. However, we also have run a series of slide-hold simulations with a much lower restitution coefficient of $\epsilon_n = 0.3$. Consistent with previous DEM studies at low sliding speeds, we find that the adopted value of the restitution coefficient appears to have very little influence on the macroscopic behavior of systems in the dense granular flow regime (Gaume et al., 2011; da Cruz et al., 2005; Silbert et al., 2001; Ferdowsi & Rubin, 2020) (see also Figure 9 of this paper). The full details of the granular module of LAMMPS are described in the LAMMPS manual and several references (Zhang &

235 Makse, 2005; Silbert et al., 2001; Brilliantov et al., 1996). Unless otherwise specified in this paper,
 236 all details of the present model, except for the values of pulling spring stiffness, are identical to the
 237 “default” model of Ferdowsi and Rubin (2020).

238 The relation of the velocity V in equations (1)–(3) to the granular simulations merits some
 239 discussion. In particular, this V is not the velocity of the upper (driving) plate. In laboratory experi-
 240 ments, slip parallel to the frictional interface is monitored between two points on opposite sides of,
 241 and some distance from, that interface, and the actual (inelastic) slip δ is estimated from

$$\begin{aligned}\delta &= \delta_{lp} - \delta_{el} = \delta_{lp} - \tau/k ; \\ \tau &= k(\delta_{lp} - \delta) .\end{aligned}\quad (4)$$

242 Here δ_{lp} is the measured “load-point” displacement, δ_{el} is the elastic distortion of the system be-
 243 tween the monitoring points resulting from stress changes, τ is the measured stress, and k is the
 244 elastic stiffness of the combined testing apparatus plus sample between the monitoring points (units
 245 of stress/distance). Taking the time-derivative of (4) leads to an estimate of the sliding speed as a
 246 function of measured quantities. Conceptually, δ in lab experiments is often treated as occurring
 247 on a discrete plane, but, just as in our numerical simulations, it actually occurs over a region whose
 248 thickness is a priori unknown.

We treat our model output in the same way. δ_{lp} is the displacement of the end of the spring at
 which the velocity is imposed, and τ is the spring force divided by the $6 \text{ cm} \times 6 \text{ cm}$ surface area
 of the driving plate. The effective stiffness k is given by treating the spring and gouge as being in
 series:

$$k = \frac{k_{sp}k_H}{k_{sp} + k_H} \quad (5)$$

249 where k_{sp} and k_H are the spring and gouge stiffness, respectively, and H denotes the gouge thick-
 250 ness. Equivalently, we could treat the “load-point” displacement δ_{lp} as being the measured displace-
 251 ment of the driving plate, in which case $k = k_H$ (showing, after insertion into (4) and differentiating,
 252 that V is not the velocity of the upper plate if the stress is changing, as this changes the elastic
 253 distortion of the gouge).

254 The shear modulus of the gouge layer can be estimated from the initially linear (nearly elastic)
 255 portion of the loading stress-strain curve at the start of a steady-sliding test. In Fig. B1 of Ferdowsi
 256 and Rubin (2020), we show the sensitivity of the gouge shear modulus to hold time duration in SHS
 257 tests, and we find that at 5 MPa $G_H \approx 270 - 310 \text{ MPa}$ regardless of hold time. From the value
 258 of shear modulus $G_H \approx 300 \text{ MPa}$, the stiffness k_H can be determined as $k_H = G_H/H = 7.3 \times 10^9$
 259 Pa/m, where $H = 0.04 \text{ m}$ is the gouge thickness. We can further determine k_{sp} in Pa/m from the
 260 spring stiffness input, k_{pull} , in LAMMPS in units of N/m, by dividing k_{pull} by the sample surface
 261 area. We use 3 pulling spring stiffnesses: $k_{pull} = 1 \times 10^{10}, 8 \times 10^5, 2.7 \times 10^4 \text{ N/m}$ corresponding
 262 to dimensionless system stiffness $\bar{k}_d \equiv kD_c/(b\sigma) \approx 425, 12, 0.4$, respectively, where the “ \approx ” sign
 263 indicates that the values of the normalizing constants b and D_c , determined from fitting simulated
 264 velocity-step tests, are known only to within about 10%. The dimensionless stiffness $\bar{k}_d \approx 425$ rep-
 265 represents the approximate upper bound for what we can achieve; $k_{pull} = 10^{10} \text{ N/m}$ is large enough that
 266 essentially all the elastic compliance comes from the gouge. The dimensionless system stiffnesses
 267 of $\bar{k}_d \approx 12$ and 0.4 were chosen to be close to the values of \bar{k} in the SHS experiments performed on
 268 the rotary shear apparatus of Beeler et al. (1994), to which we compare some of our granular model
 269 observations. After performing the granular simulations reported in this work, our estimates of \bar{k}_d
 270 for those lab data, based on the analysis of Bhattacharya et al. (2021), were reduced by 1/3 from
 271 their initial values, to $\bar{k}_d \approx 8$ and 0.27 , so the match with our simulations is not exact. For analysis
 272 of our simulation data we used values of $D_c = 1.77D_{mean} = 0.0053 \text{ m}$, $a = 0.0247$, and $b = 0.0178$
 273 which were obtained from velocity-stepping simulations (Ferdowsi & Rubin, 2020).

274 Friction in our simulations is defined as the ratio of the shear to normal force exerted on the
 275 upper rigid block by the gouge grains in contact with it. If accelerations of the upper plate are unim-
 276 portant, this shear force can be equated with the force applied by the pulling spring in (4). If the
 277 plate velocity suddenly changes to or from $\sim 1 \text{ m/s}$, this assumption is violated and wave propagation

278 within the gouge must be considered (Ferdowsi & Rubin, 2020, Appendix B). The SHS simulations
 279 reported here were run with initial steady-state velocities of $V_i = V_{Ip} = 2 \times 10^{-3}$, 2×10^{-2} , and
 280 10^{-1} m/s, and in most simulations we used a reslide velocity equal to the initial velocity. However,
 281 in a small number of cases we changed the reslide velocity to search for deviations from the pre-
 282 dictions of existing RSF equations; any such deviations would be relevant to models of earthquake
 283 nucleation. We also performed a series of slide-hold simulations at the smaller initial sliding veloci-
 284 ty of $V_i = 2 \times 10^{-4}$ m/s. In laboratory experiments, the sliding velocity is typically on the order
 285 of $1 - 10 \mu\text{m/s}$; however, running simulations at such velocities is not yet possible with the DEM
 286 method within reasonable computational costs, provided one uses grain elastic properties and den-
 287 sities appropriate for quartz-like materials. Our fully parallelized simulations at sliding velocities of
 288 $V_i = 2 \times 10^{-2}$, 2×10^{-3} and 2×10^{-4} m/s, took about a few days, two weeks, and six weeks of real
 289 time, respectively, to achieve steady-state friction on Princeton’s PICSciE’s computational cluster.
 290 The longest holds took 5 months.

291 To assess the importance of our deviation from lab-like parameters, we turn to dimensionless
 292 ratios. The sliding velocity enters only one – the Inertial number, a critical parameter in granular
 293 flows, defined as $I_n \equiv \dot{\gamma} D_{mean} \sqrt{\rho/P} \approx V(D_{mean}/H) \sqrt{\rho/P}$, where $\dot{\gamma}$ is the local shear rate, the
 294 approximate equality is appropriate for our loading geometry (we do not see localization in our
 295 system), P is the confining pressure (synonymous with the normal stress in these simulations), and ρ
 296 and D_{mean} are the density and mean diameter of grains, respectively. The inertial number measures
 297 the ratio of the inertial forces of grains to the confining forces acting on those grains, such that
 298 small values ($I_n \lesssim 10^{-3}$) correspond to the dense, quasi-static regime of shearing that we desire to
 299 model (da Cruz et al., 2005; Forterre & Pouliquen, 2008). The SHS simulations reported here with
 300 $V_i = 2 \times 10^{-3}$ to 10^{-1} m/s have inertial numbers during steady sliding satisfying $\sim 10^{-6} \lesssim I_n \lesssim 10^{-4}$,
 301 all in this quasi-static regime. Ferdowsi and Rubin (2020) explore the range $\sim 10^{-7} \lesssim I_n \lesssim 10^{-3}$
 302 during velocity-step tests, and find no significant variation in the RSF parameter values. There is no
 303 a priori expectation that the RSF parameters will begin to vary at still lower I_n , but of course one does
 304 not know this, and testing for systematic changes with V_i provides the motivation for performing
 305 SHS tests at a range of achievable sliding velocities within the quasi-static regime.

306 Confining pressure enters the Inertial number discussed above as $P^{-1/2}$, and also the “dimen-
 307 sionless pressure” $\bar{P} = (P/E)^{2/3}$, where E is Young’s modulus (50 GPa in our simulations). \bar{P} is
 308 a measure of the grain strain at the imposed confining pressure; the $2/3$ power is appropriate for
 309 contacting elastic spheres (Hertzian contacts). With $P = 5$ MPa, $\bar{P} = 2 \times 10^{-3}$ in our simulations.
 310 Ferdowsi and Rubin (2020) explored values $0.7 \times 10^{-3} \lesssim \bar{P} \lesssim 6 \times 10^{-3}$ ($1 < P < 25$ MPa), and found
 311 only modest variations in the RSF parameter values. Rather than tailor our values of \bar{P} to individual
 312 experiments, we chose to maintain the default value of $P = 5$ MPa in Ferdowsi and Rubin (2020),
 313 and rely on their observation that the RSF parameters do not seem to be very sensitive to this choice.

314 In contrast, there is reason to believe that the choice of system stiffness in our slide-hold and
 315 SHS simulations is quite important. For the longest (load-point) holds conducted by Beeler et al.
 316 (1994), one can estimate (from their reported stress drops and stiffnesses) that there was $\sim 2.4 \mu\text{m}$
 317 of accumulated slip in their high-stiffness case and $\sim 16 \mu\text{m}$ of slip in their low-stiffness case. For
 318 $D_c \sim 2 \mu\text{m}$ (Bhattacharya et al., 2021) this corresponds to roughly $1.2D_c$ and $8D_c$ of slip. Given the
 319 potential importance of slip on the order of D_c to state evolution, this difference is quite significant.
 320 For a complete list and discussion of the governing dimensionless variables of the model, see Ap-
 321 pendix A of Ferdowsi and Rubin (2020). As one last point, we note that reducing all length scales
 322 (the grain size and all model dimensions) by the same factor, while keeping V_i the same, results in
 323 simulations that are dimensionally identical.

324 4 Results and discussion

325 4.1 General considerations

326 Before proceeding to the results of the granular simulations, it is worth considering what it
 327 means to “compare” our results to laboratory experiments. The ratio a/b for the granular simulations,

328 determined from simulated velocity steps, is ~ 1.4 , and may be fixed by our choice of spherical
 329 particles, Gaussian-like grain size distribution, and the tangential and normal contact laws we have
 330 adopted (for example, Ferdowsi and Rubin (2020) found that a more exponential-like grain size
 331 distribution gave rise to simulations with values of a/b much closer to 1; we did not pursue those here
 332 because they were noisier and would have required even larger system sizes and more computational
 333 resources to see clear signals). The value $a/b \sim 1.4$ is slightly high by lab standards, and we are
 334 not aware of lab experiments that push surfaces with such values far enough from steady state to
 335 be useful for constraining models of state evolution. Therefore we do not necessarily expect our
 336 granular simulations to match any particular lab experiment. Nonetheless, we were able to claim that
 337 the simulations successfully capture the phenomenology of laboratory velocity-step experiments.
 338 This phenomenology entails that the amplitudes of the changes in friction with velocity and state are
 339 proportional to the logarithm of the velocity step (amplitudes controlled in RSF by the parameters
 340 a and b), and that friction evolves to its future steady state value over a characteristic slip distance
 341 (D_c), independent of the size or sign of the velocity step. Because, by design, these attributes of lab
 342 experiments are replicated by the Slip version of the RSF equations, it was convenient to use Slip
 343 law fits to our simulation output to determine the values of a , b , and D_c that fit our data well (note
 344 that absent some conceptual model for friction, we could not even have made the statement above
 345 that in our simulations “ $a/b \sim 1.4$ ”).

346 For slide-hold tests the situation is more complicated, because it is less obvious what the “phe-
 347 nonomenology” of laboratory holds is. Here we made more essential use of comparisons between
 348 our simulations and the predictions of the Aging and Slip laws for state evolution, on the one hand,
 349 and comparisons between the Aging and Slip laws and laboratory experiments, on the other. Bhat-
 350 tacharya et al. (2017; 2021) showed that the stress decay during laboratory holds was fit reasonably
 351 well by Slip law simulations, using parameter values determined independently from velocity steps,
 352 and that the Aging law, with its time-dependent healing, predicted too little stress decay. Because
 353 these features of the lab data were replicated by our numerical simulations, we used this indirect
 354 comparison (granular simulations to RSF / RSF to lab data) to claim that the granular simulations
 355 also seemed to do a good job matching laboratory slide-hold experiments (although, as we noted
 356 previously, the comparison in Ferdowsi and Rubin (2020) was made using a system stiffness that
 357 exceeds those achievable in the lab). For SHS tests, the salient phenomenology is that the peak
 358 friction upon resliding increases nearly linearly with the logarithm of hold time. For the Aging law,
 359 which was designed to produce this behavior, the slope of this increase (suitably normalized) is the
 360 RSF parameter b , whereas in lab experiments it seems to be variable but roughly a factor of 2 smaller
 361 (see Section 4.3). So although in this case we could “compare” the slope in our simulations directly
 362 to lab data without seeming to reference the Aging law, in fact by choosing to compare the slope to
 363 b we are implicitly making use of the Aging law. That is, absent some moderately successful model
 364 prediction, it is not apparent what we should be comparing the slope of our healing relation to.

365 4.2 Slide-hold simulations

366 In this section we present the slide-hold (SH) behavior of the granular model. Since individual
 367 simulations tend to be somewhat noisy, all simulation signals presented in this manuscript are aver-
 368 aged over eight different realizations (initial grain arrangements) of the model, all subjected to the
 369 same boundary conditions. Friction is defined as the ratio of shear to normal stress τ/σ , where τ
 370 is the shear force per unit area exerted by the gouge particles on the upper (driving) plate, and σ is the
 371 normal force per unit area on the upper plate.

372 Figures 2a-c show the variation of normalized friction with normalized hold time for SH tests,
 373 with initial sliding velocities of $V_i = 2 \times 10^{-3}$, 2×10^{-2} , and 10^{-1} m/s shown by the cyan, blue,
 374 and black curves, respectively. Panel (a) shows the results of simulations run with system stiffnesses
 375 $\bar{k}_d \approx 425$, while panels (b) and (c) show simulations with system stiffness $\bar{k}_d \approx 12$ and $k_d \approx 0.4$,
 376 respectively. Based on the indicated reductions in friction and the system stiffnesses, the longest
 377 holds in these simulations correspond to total (inelastic) slips within the gouge layer of roughly
 378 (from most to least stiff) $0.04D_c$, D_c , and $10D_c$.

379 Lowering the stiffness delays the onset of stress decay because a given stress reduction then
 380 requires a longer slip distance; at constant sliding velocity, elasticity dictates that the normalized
 381 friction change $\Delta\mu/b$ reaches -1 when $t_{hold}/(D_c/V_i) = \bar{k}^{-1}$, which is roughly when the stress tra-
 382 jectories in Figure 2 leave their initial plateau (the Slip law predictions for $\bar{k}_d \approx 12$ and $\bar{k}_d \approx 0.4$
 383 have been included in panel (a) for reference). From dimensional analysis, standard RSF (equations
 384 1–3 with constant parameter values) predicts that the curves for the same \bar{k} but different V_i overlap
 385 identically when plotted versus dimensionless hold time $\bar{t}_{hold} \equiv t_{hold}/(D_c/V_i)$. Our simulations at
 386 the three sliding velocities with $\bar{k}_d \approx 425$ show a stress decay response that is not exactly the same,
 387 but they are nevertheless similar to each other within their standard deviations. The stress decay
 388 response for the three velocities differ more significantly at the lower stiffnesses of $\bar{k}_d \approx 0.4$ and 12.

389 Figures 2a-c also include the predictions of the Aging and Slip laws for the stiffnesses used
 390 in the granular model. These predictions are obtained using the RSF parameter values determined
 391 independently from Slip law fits to simulated velocity steps performed on the identical granular
 392 system (Ferdowsi & Rubin, 2020). For $\bar{k}_d \approx 425$, the stress decay of the granular model is in
 393 excellent agreement with the Slip law prediction. There is also reasonable agreement for the lower
 394 stiffnesses of $\bar{k}_d \approx 0.4$ and 12, where the Slip law prediction generally lies between the curves for
 395 the different V_i (we return to the differences between the different V_i below). In contrast, for the
 396 two larger stiffnesses, where the Aging- and Slip-law predictions differ, the Aging-law significantly
 397 underestimates the stress decay at long hold times. The shallowing slope of the stress decay for
 398 the Aging law results from its prediction of continual state evolution, $\dot{\theta} \approx 1$ in equation 2, even at
 399 vanishing slip rates. Analytically, the slope of the stress decay at long hold times for the Aging law
 400 (with $a/b > 1$) is $(1 - a/b)$ when plotted vs. $\ln(\bar{t}_{hold})$, and $2.3(1 - a/b)$ when plotted vs. $\log_{10}(\bar{t}_{hold})$,
 401 independent of the system stiffness (Bhattacharya et al., 2017, Appendix C). For the Slip law, the
 402 long-time slope in general depends upon stiffness, but in the “infinite-stiffness limit” it is $2.3(-a/b)$
 403 when when plotted vs. $\log_{10}(\bar{t}_{hold})$ (Bhattacharya et al., 2017), which for the parameter values of
 404 our granular simulations is 3.6 times larger. All 3 initial velocities for $\bar{k} \approx 425$ in Figure 2a, and the
 405 corresponding Slip-law prediction, have this “infinite-stiffness limit” slope. For $\bar{k}_d = 0.4$, there is
 406 sufficiently little reduction in slip speed that the predictions of the Aging and Slip laws are extremely
 407 similar.

408 Because our initial sliding velocities are higher than those typically used in laboratory slide-
 409 hold experiments, it is important to assess any systematic trends with V_i in the granular simulations.
 410 At the highest stiffness ($\bar{k} \approx 425$), the curves for the different V_i tend to weave around the Slip-law
 411 prediction, but they all end up with the same (Slip-law) slope at the longest hold times. At short
 412 hold times for $\bar{k} \approx 12$ and 0.4, there do not seem to be trends that are monotonic with V_i , with the
 413 slowest velocity (2×10^{-3} m/s) plotting between the two larger velocities. However, at the longest
 414 hold times in Figure 2b ($\bar{k} \approx 12$), there is a systematic trend of lower stress with lower V_i . Whether
 415 this trend would persist to longer hold times is not known.

416 An example of frictional behavior during a laboratory slide-hold experiment on rock is shown
 417 in Fig. 2d, from Bhattacharya et al. (2021). The experiment was performed on a granite sample with
 418 initial sliding velocity $V_i = 0.316 \mu\text{m/s}$, system stiffness $\bar{k}_d \approx 8$, and confining stress 25 MPa. The
 419 Aging and Slip law predictions for the experiment are shown with green and pink lines, respectively.
 420 These predictions, similar to the RSF predictions for the granular model, are obtained using the RSF
 421 parameter values determined independently from Slip law fits to velocity-stepping experiments on
 422 the same sample. Overall, as with the fits to the granular simulations, they indicate that the Aging
 423 law underestimates the stress decay in the lab at long hold times, while the Slip law provides a very
 424 good prediction of the behavior. Comparing the behavior of both the lab data and the granular model
 425 to the Aging and Slip law predictions, especially Figures 2b and 2d with close to the same stiffness,
 426 we conclude that although the stress decay in the simulations is not strictly log-linear as for the lab
 427 data, the granular model qualitatively captures the stress decay observed in laboratory slide-hold
 428 tests.

429 The stress decay during slide-hold protocols clearly rules out the Aging law for the evolution
 430 of state in both the granular model and laboratory experiments. This is despite the fact that log-
 431 time fault-normal compaction is almost universally observed during laboratory holds under room-

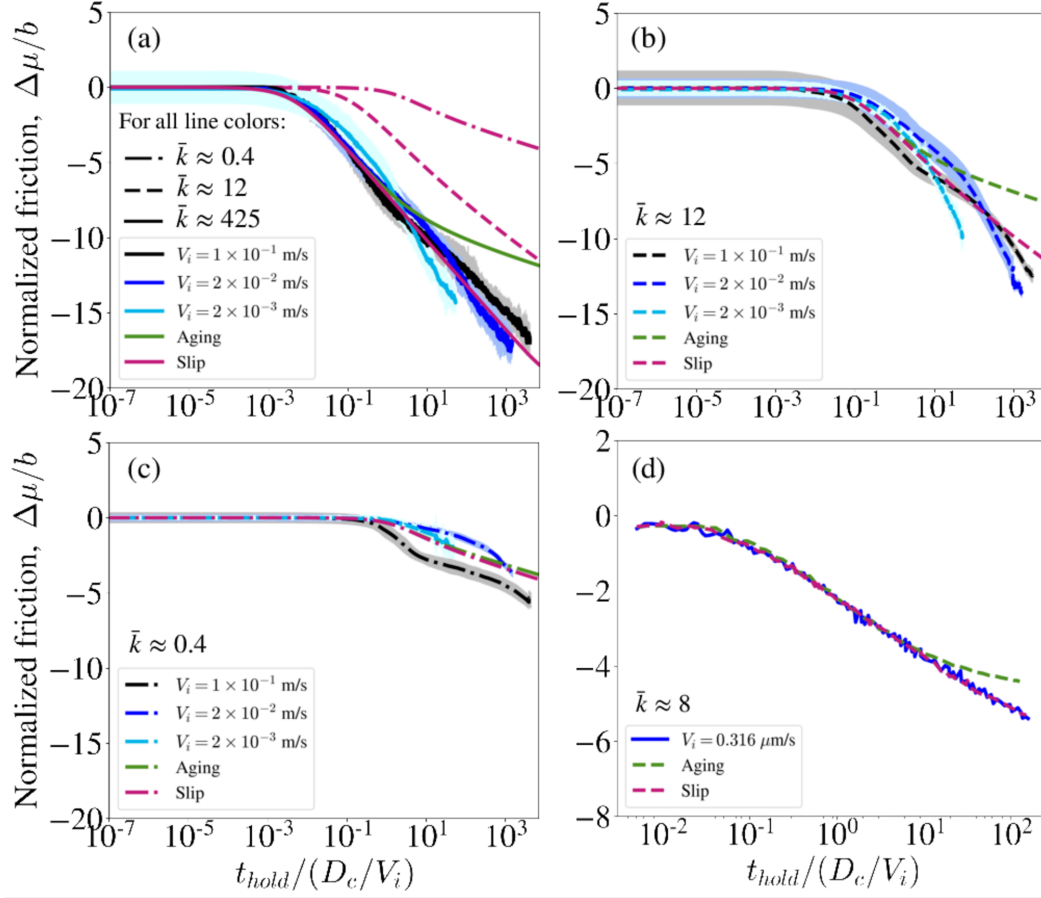


Figure 2. The slide-hold behavior: The cyan, blue, and black lines in panels (a-c) show the variation of friction coefficient, normalized by the RSF parameter b , as a function of normalized hold time, for granular slide-hold simulations with prior sliding velocities V_i of 2×10^{-3} (cyan), 2×10^{-2} (blue), 10^{-1} (black) m/s. Panels (a), (b), and (c) show the behavior of the systems with stiffness $\bar{k}_d \approx 425$, 12, and 0.4, respectively. The pink and green lines in panels (a-c) further show the predictions of the Slip and Aging laws, respectively, using the RSF parameters ($D_c = 0.0053$ m, $a = 0.0247$, $b = 0.0178$) determined independently from Slip-law fits to velocity-step tests performed on the same model (Ferdowsi & Rubin, 2020). The predictions of the Slip and Aging laws are shown with different line styles for different system stiffnesses (the Slip law predictions for $\bar{k} = 12$ and 0.4 are included in panel (a) only for reference). Granular simulation results in panels (a-c) are averaged over 8 different realizations (initial grain arrangements) subjected to the same imposed loading conditions. Black, blue, and cyan lines show the mean behavior of the realizations for each system, and the width of the gray, blue, and cyan shades around each line shows the 2-sigma deviations. The confining pressure in all simulations is 5 MPa. (d) The blue line shows the variation of friction coefficient, normalized by the RSF parameter b , as a function of normalized hold time, for an experiment performed in the Tullis rotary shear apparatus at Brown University on a granite sample with prior sliding velocity $V_i = 0.316 \mu\text{m/s}$. The system stiffness for this experiment is $\bar{k}_d \approx 8$, and the confining stress is 25 MPa. As in panels (a-c), the pink and green lines show predictions of the Slip and Aging laws, respectively, using the RSF parameters ($D_c = 2 \mu\text{m}$, $a = 0.013$, $b = 0.016$) obtained from Slip-law fits to velocity-step tests on the same experimental sample. We used the same RSF parameters to calculate the dimensionless stiffness \bar{k} for the lab data.

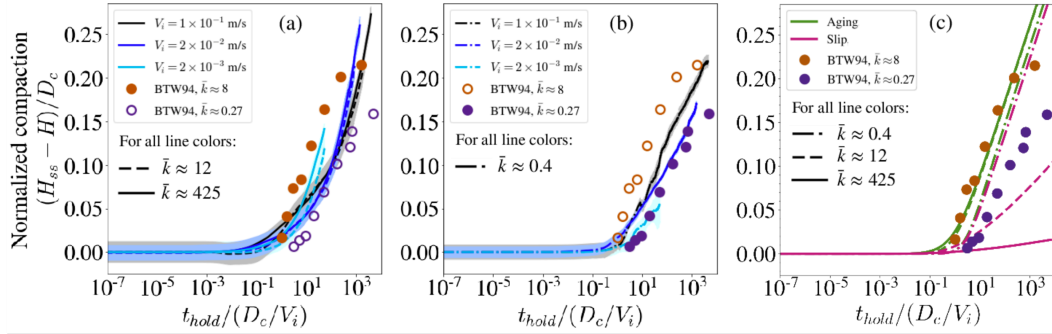


Figure 3. Gouge compaction during slide-holds: The cyan, blue, and black lines in panels (a) & (b) show the variation of gouge compaction, normalized by the RSF characteristic slip distance D_c , as a function of normalized hold time, for granular slide-hold simulations with prior driving velocities V_i of 2×10^{-3} (cyan), 2×10^{-2} (blue), and 10^{-1} (black) m/s. Panel (a) shows the behavior for stiffnesses $\bar{k}_d \approx 425$ and 12, while panel (b) shows the behavior of stiffness $\bar{k}_d \approx 0.4$. The widths of the gray, blue, and cyan shades around the mean behavior lines indicate 2-sigma deviations. (c) The pink and green lines show the evolution of $\log(\text{state})$ under the Slip and Aging laws, respectively, using the RSF parameters determined independently from Slip-law fits to velocity-step simulations (Ferdowsi & Rubin, 2020). The state evolutions are scaled by the factor $-d(H_{ss}/D_c)/d \log \theta \approx 0.035$ (Fig. 2c in Ferdowsi and Rubin (2020)), where the H_{ss} is the steady-state thickness of the granular layer (see text for discussion). Different line styles correspond to different system stiffnesses as described in the legend. The filled and empty dots in all panels show the change in gouge thickness during hold experiments on a granite sample reported by Beeler et al. (1994), who used two different ($\bar{k}_d \approx 8$ and 0.27) machine stiffnesses. The dots are filled or empty in panels (a) and (b) depending on the machine stiffness that is most appropriate to compare the granular model behavior to in that panel. An estimated slip-weakening distance $D_c \approx 2 \mu\text{m}$ is used to normalize compaction data in laboratory experiments (Bhattacharya et al., 2021). The lab experiments with stiffness $\bar{k}_d \approx 0.27$ and 8 were performed with sliding velocities $V_i = 1 \mu\text{m/s}$ and $0.32 \mu\text{m/s}$, respectively. Both low and high stiffness laboratory experiments were performed at 25 MPa confining pressure.

432 humidity conditions. This compaction is thought to be consistent with an Aging law-like evolution
 433 of state; that is, in theoretical justifications of the Aging law, the same mushrooming of highly-
 434 stressed contacts that is considered to be responsible for log-time increase of true contact area and
 435 frictional strength, would also lead to log-time compaction (Berthoud et al., 1999; Sleep, 2006).
 436 The same argument would suggest that if the stress data during holds is well modeled by the Slip
 437 law, with its relative lack of state evolution, the fault-normal compaction would be much less. This
 438 potential conflict between the stress and fault-normal displacement data from laboratory holds was
 439 noted previously by Bhattacharya et al. (2017).

440 In our previous work, we observed that in addition to matching the stress decay during labora-
 441 tory holds, the granular model led to log-time reduction in gouge thickness for $\bar{k}_d \approx 425$ (Ferdowsi
 442 & Rubin, 2020). Here we examine the changes in gouge thickness during slide-holds using stiff-
 443 nesses more appropriate for lab experiments. Figure 3a shows the gouge compaction with hold time
 444 in the granular model with stiffnesses $\bar{k}_d \approx 425$ and 12, in comparison to the gouge compaction
 445 observed in the laboratory for two system stiffnesses $\bar{k}_d \approx 8$ (filled circles) and 0.27 (lab data from
 446 Beeler et al. (1994), as reported by Bhattacharya et al. (2017)). The lab experiments were performed
 447 in a rotary shear apparatus, so there is no need to correct for sample dilation/compaction due to
 448 a Poisson effect as the loading stress changes (Beeler et al., 1996). The gouge compaction in the
 449 granular model with the lower stiffness $\bar{k}_d \approx 0.4$ is shown separately in Fig. 3b for clarity, where
 450 now the lab data for $\bar{k}_d \approx 0.4$ are shown as filled circles. These plots indicate that the magnitude

451 of gouge compaction in the granular model is in general agreement with laboratory observations,
 452 after both are normalized by their appropriate value of D_c . For the granular simulations this is the
 453 sensible normalization; Ferdowsi and Rubin (2020) found that the ratio of gouge thickness changes
 454 to D_c was independent of the nominal gouge thickness over the range they explored. For the lab
 455 data, normalization by D_c is intended to account for the fact that deformation is typically localized
 456 over a layer of unknown thickness; inherent in this approach is the assumption that both slip and
 457 compaction are concentrated within this layer. Together, panels (a) and (b) show that gouge com-
 458 paction in the granular model is much less strongly dependent on system stiffness than is the stress
 459 decay, and that the normalized rate of compaction with log time is close to that of the lab data (most
 460 obviously for the simulation with lowest stiffness, panel (b), which is also the simulation for which
 461 the compaction is most nearly log-linear). The lab data show more of a stiffness-dependent offset
 462 along the time axis than do the simulations, although the simulations with the lowest V_i of 2×10^{-3}
 463 m/s show a modest offset of the proper sign.

464 The relatively weak dependence of the compaction rate on stiffness in the granular simulations
 465 is reminiscent of the Aging-law prediction for the evolution of state θ , because for long Aging-law
 466 holds $\dot{\theta} \sim 1$, independent of all else. Fig. 3c shows the evolution of $\log(\text{state})$ as predicted using
 467 the RSF Aging and Slip laws (in green and red, respectively), for the three stiffnesses used in the
 468 granular model. To plot $\log(\text{state})$ on the same axis as compaction, we use the linear relation between
 469 steady-state gouge thickness and log velocity found by Ferdowsi and Rubin (2020), combined with
 470 the RSF relation that at steady state velocity is inversely proportional to state. That is, we multiply
 471 the computed change in $\log(\text{state})$ by the factor $-d(H_{ss}/D_c)/d \log \theta$, found to be ~ 0.035 in Figure
 472 2c of their paper, where H_{ss} is the steady-state thickness of the gouge layer. The agreement between
 473 this Aging law prediction and the lab data, and from comparison to Figures 3a and 3b the agreement
 474 between the granular simulations and the lab data, is quite remarkable. The evolution of state under
 475 the Slip law for the lowest stiffness is, as with the stress decay, very similar to that for the Aging law.
 476 However, as the system stiffness increases, the evolution of state under the Slip law significantly
 477 decreases because the amount of slip decreases. Translating this state evolution to fault-normal
 478 compaction as in Figure 3c, the prediction would be that compaction for the Slip law should be
 479 strongly stiffness-dependent, completely unlike compaction in the simulations and in the lab data.
 480 All of this serves to emphasize the point that while stress during the holds is fit well by the Slip law,
 481 compaction during the holds is fit much better by the Aging law prediction of state evolution.

482 4.3 Slide-hold-reslide simulations

483 We have thus far presented a detailed discussion of the slide-hold behavior of the granular
 484 simulations. A main motivation for conducting SHS experiments on rock is to better understand
 485 the fault healing that occurs during interseismic intervals, healing that is necessary for repeated
 486 earthquakes to occur on the same section of fault. This healing historically has been measured
 487 by the peak stress $\Delta\mu_{peak}$ upon resliding following a hold (see the inset in Figure 4a), under the
 488 assumption that little state evolution occurs in the short time or slip distance between the start of
 489 the reslide and the peak stress (we leave aside here the question of whether room temperature and
 490 humidity experiments are relevant to natural faults at depth). Because the Aging law embodies fault
 491 healing (state evolution) with time even in the absence of slip, for the same parameter values it
 492 generates more healing during holds than the Slip law. More diagnostically, sufficiently long hold
 493 times lead to $V\theta/D_c \ll 1$, so from equation 2 for the Aging law, $\dot{\theta} \approx 1$. This means that for long hold
 494 times the rate of healing with log hold time is independent of how much slip accumulates during
 495 the hold, and hence it is independent of the elastic stiffness of the loading system (Beeler et al.,
 496 1994; Bhattacharya et al., 2017). These authors further showed that the Aging law predicts that the
 497 reduction in $\log(\text{state})$ between the start of the reslide and peak stress is independent of hold duration,
 498 and hence that the predicted change in peak friction with log hold time, $d\Delta\mu_{peak}/d \ln(\bar{t}_{hold})$, equals
 499 the RSF parameter b (equation (1); note that at peak stress $d\tau/dt = 0$, so from elasticity the sliding
 500 velocity equals the load-point velocity). This property was exploited by Beeler et al. (1994), who ran
 501 lab experiments with two loading machine stiffnesses and found that, indeed, for long hold times,
 502 the rate of healing was independent of stiffness. Bhattacharya et al. (2017) later showed that, for
 503 the two stiffnesses and hold durations of those experiments, the same stiffness-independent rate of

504 healing could be achieved by the Slip law, but over a more restricted range of RSF parameters. Those
 505 parameters do not include the ratio of a/b appropriate for our granular simulations.

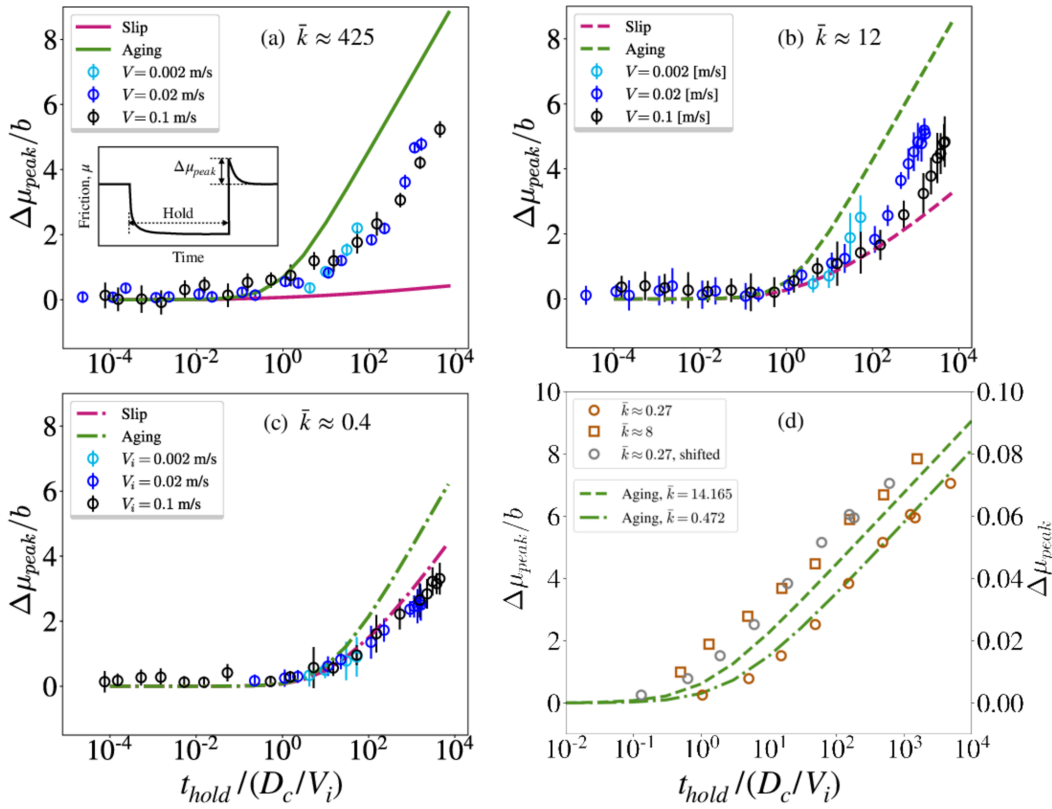


Figure 4. Frictional healing in the granular model: Solid circles show $\Delta\mu_{peak}$ normalized by the RSF parameter b (estimated from velocity steps), as a function of normalized hold time in granular slide-hold-slide simulations at $V_i = 2 \times 10^{-3}$, 2×10^{-2} , and 10^{-1} m/s. Panels (a), (b), and (c) show the results for system stiffnesses of $\bar{k}_d \approx 425$, 12, and 0.4, respectively. Error bars are 2-sigma deviations of 8 different realizations. The green and pink lines in each panel show the predictions of the Aging and Slip laws, respectively, for that specific system stiffness using the RSF parameters obtained from velocity-step tests. The inset in panel (a) shows the schematic of a slide-hold-slide test and the definition of frictional healing, $\Delta\mu_{peak}$. (d) Frictional healing in the lab: Solid circles show $\Delta\mu_{peak}$ as a function of normalized hold time, in slide-hold-slide experiments performed on a granite sample at 25 MPa confining pressure (Beeler et al., 1994) with machine stiffness $\bar{k}_d \approx 0.27$ and 8, at sliding velocities of $V_i = 1 \mu\text{m/s}$ and $0.32 \mu\text{m/s}$, respectively. The green dashed lines show the evolution of frictional healing, $\Delta\mu_{peak}$, normalized by the RSF parameter $b = 0.0109$ (estimated from the slope of healing vs. time data in this figure) with $a - b = -0.0027$ (Bhattacharya et al., 2017) and $D_c = 2 \mu\text{m}$ (Bhattacharya et al., 2021). These parameters result in normalized stiffness values of $\bar{k}_d \approx 0.472$ and 14.165 for the Aging law predictions in this plot.

506 It is well established from decades of laboratory experiments on rock and gouge that the peak
 507 friction upon resliding increases nearly linearly with log hold time (J. H. Dieterich, 1972; Beeler et
 508 al., 1994; Baumberger & Caroli, 2006; Marone & Saffer, 2015; Carpenter et al., 2016). The only
 509 study of which we are aware that compares the observed rate of increase to the Aging law prediction,
 510 $d\Delta\mu_{peak}/d\ln(\bar{t}_{hold}) = b$, using values of b determined independently from velocity-step tests, is the
 511 combined work of Ikari et al. (2016) and Carpenter et al. (2016) on natural and synthetic gouge
 512 materials. Excluding their synthetic clay gouges, for which our granular simulations with spherical

513 grains are likely inappropriate, Ikari et al. (2016) found slopes mostly in the range of $\sim 0.3b$ to $0.7b$.
 514 Beeler et al. (1994) found $d\Delta\mu_{peak}/d\ln(\bar{t}_{hold}) \sim 0.01$ for their granite sample, close to the expected
 515 value of b for granite, but a slope of ~ 0.004 for quartzite, probably a factor of ~ 2 lower than the
 516 expectation for b . Marone and Saffer (2015) found slopes of ~ 0.0035 , plus or minus several tens of
 517 percent depending upon V_i , values that seem within the range of Ikari et al. (2016).

518 Beyond this, results seem to be limited to single studies. As mentioned previously, Beeler et al.
 519 (1994) showed that the rate of frictional strengthening $d\Delta\mu_p/d\ln(\bar{t}_{hold})$ was independent of system
 520 stiffness, and interpreted this as suggesting that frictional healing depends upon time rather than slip.
 521 Marone and Saffer (2015) showed that the rate of frictional strengthening in their synthetic gouge
 522 samples depended upon V_i , increasing by nearly a factor of 2 over the range 1–100 $\mu\text{m/s}$, indica-
 523 tive of a velocity-dependence of the RSF parameters or a characteristic velocity in the governing
 524 equations not captured by the standard RSF equations (1)–(3). However, over the same range of
 525 velocities Carpenter et al. (2016) found no significant dependence upon V_i .

526 Here we present results of granular SHS simulations for a wide range of hold times at $V_i =$
 527 2×10^{-3} , 2×10^{-2} , and 10^{-1} m/s. Panels (a), (b) and (c) in Fig. 4 show the changes in peak stress
 528 with hold time for simulations performed with stiffnesses $\bar{k}_d \approx 425$, 12, and 0.4, respectively.
 529 These panels show that for the longest holds, the peak stress increases nearly logarithmically with
 530 hold time, in qualitative agreement with laboratory rock friction data. In each panel the green and
 531 red lines indicate the predictions of Aging and Slip law simulations, respectively, using parameter
 532 values determined from Slip law fits to our velocity-step simulations. For each stiffness (each panel)
 533 the slope of the green Aging-law prediction is equal to b , when plotted vs. $\ln(\bar{t}_{hold})$ rather than
 534 $\log_{10}(\bar{t}_{hold})$. Comparison to the granular simulations show that the slope of the log-time healing
 535 ranges from $\sim 0.5b$ to b , also in qualitative agreement with laboratory data. However, unlike the data
 536 of Beeler et al. (1994), the rate of healing at long hold times differs by nearly factor of 2 between
 537 the simulations with $\bar{k} \approx 12$ and $\bar{k} \approx 0.4$. In addition, unlike the data of Marone and Saffer (2015),
 538 but similar to that of Carpenter et al. (2016), there is not an obvious dependence of this slope upon
 539 V_i .

540 In contrast to the Aging law, the Slip law simulations produce a strongly stiffness-dependent
 541 rate of frictional healing. For $\bar{k} \approx 425$, there is so little slip that there is almost no state evolution
 542 (healing). For $\bar{k} \approx 0.4$, there is so much slip that the rate of healing is not much less than that for
 543 the Aging law. Note that the healing in the granular simulations is more than that predicted by the
 544 Slip law when $\bar{k}_d \approx 425$ and 12, but less than predicted when $\bar{k}_d \approx 0.4$. Thus, the observation of
 545 Ferdowsi and Rubin (2020) that for $\bar{k} \approx 425$ the healing in the granular model lies between the
 546 Aging and Slip law predictions is not generalizable to all stiffnesses.

547 The laboratory rock friction data of Beeler et al. (1994) are shown in Figure 4d. Only $(a - b)$
 548 was determined in this study, so for the Aging law simulations shown we take $D_c = 2\mu\text{m}$ determined
 549 for the same sample by Bhattacharya et al. (2021), and fix $b = 0.0109$ to match the slope of the
 550 lab healing curves. This comparison shows that while healing in the lab data leads that of the
 551 Aging law prediction (for the higher lab stiffness) or is in general agreement with it (for the lower
 552 stiffness), healing in the granular simulations generally lags the corresponding Aging-law prediction.
 553 This comparison should be extended to experiments where the RSF parameters were determined
 554 independently.

555 In laboratory slide-hold-slide experiments, the reslide is accompanied by dilation of the gouge
 556 layer, dilation that continues monotonically beyond the moment of peak stress to the future steady-
 557 state thickness. We observe the same behavior in our simulations. Figures 5a to 5c show the variation
 558 of dilation at peak stress in the granular model for the sliding velocities $V_i = 0.1$, 0.02, and 0.002
 559 m/s, respectively, for each of the 3 stiffnesses we used. This dilation increases nearly linearly with
 560 log-hold time. For the simulations with $V_i = 0.1$ and 0.02, the magnitude of this dilation (at large
 561 normalized hold times) decreases with increasing system stiffness, opposite to the trend seen in the
 562 lab data of Beeler et al. (1994) and shown in Fig. 5d. The trend of the change in dilation at peak
 563 stress with system stiffness for the simulations with $V_i = 0.002$ m/s is in better agreement with the
 564 laboratory observations in Fig. 5d. We further normalize the dilation at peak stress by the amount

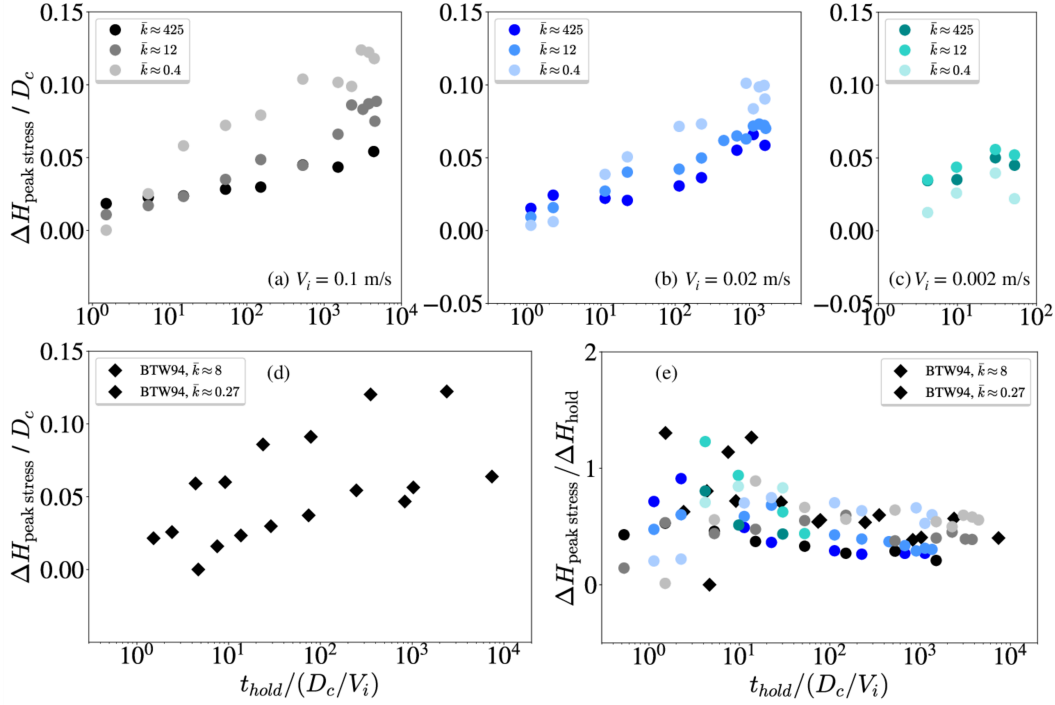


Figure 5. The variation of normalized dilation at peak stress ($\Delta H_{\text{peak stress}}/D_c$) versus hold time, following reslides for the granular model with sliding velocities of (a) $V_i = 0.1$ m/s, (b) $V_i = 0.02$ m/s, and (c) $V_i = 0.002$ m/s. The amount of dilation is defined as the change in gouge thickness between the end of the hold and the moment of peak stress, as in Fig. B1 of Bhattacharya et al. (2017). The simulations are performed at three different stiffnesses and 5 MPa confining stress. (d) dilation at peak stress ($\Delta H_{\text{peak stress}}$) in the lab (data of Beeler et al. (1994)), (e) The ratio of dilation at peak stress ($\Delta H_{\text{peak stress}}$) to compaction at the end of the corresponding hold in the granular model (circles) and in the lab (diamonds) (data of Beeler et al. (1994)). The lab data shown in panels (d) and (e) are reported by Bhattacharya et al. (2017).

565 of compaction at the end of the corresponding hold. The ratio of dilation/compaction that results
 566 from this analysis is shown in Fig. 5e, plotted alongside the same quantity observed in the lab
 567 data of Beeler et al. (1994). Comparing the lab data to the simulations conducted at roughly the same
 568 stiffnesses, we find that the relative slopes of the log-linear portion of the dilation and compaction in
 569 both the simulations and lab (normalized hold times $\gtrsim 10^1$) are in the fairly narrow range ~ 0.4 – 0.5 ,
 570 and are therefore in qualitative agreement with each other. For shorter hold times, both the lab
 571 data and simulations show considerable scatter.

572 Among other features observed in slide-hold-slide tests, Figure 5 of Marone and Saffer (2015)
 573 suggests that the slip-weakening distance following the peak stress upon resliding increases with
 574 hold duration. This feature is inconsistent with the Slip law prediction, but we see evidence of
 575 similar behavior in our SHS simulations. Figures 6a & b show the variation of friction coefficient
 576 with sliding distance in the reslide portion of SHS simulations performed after a range of hold times,
 577 for $V_i = 0.1$ and 0.02 m/s, referenced to the steady-state friction value at V_i . These signals show
 578 (more obviously in Fig. 6a) that the slip distance to peak friction increases with increasing hold time,
 579 as for the Marone and Saffer (2015) data (their Figure 12). Panels c-d in Fig. 6 also include the Slip
 580 law prediction for a one-order velocity-step increase, normalized to the same peak-residual value as
 581 the reslide friction signals. These two panels more clearly demonstrate the increase in weakening
 582 distance with hold time. The reslides at shorter holds have a weakening distance, D_c , roughly equal
 583 to the distance observed in the velocity-steps. At longer hold times, D_c further increases, although

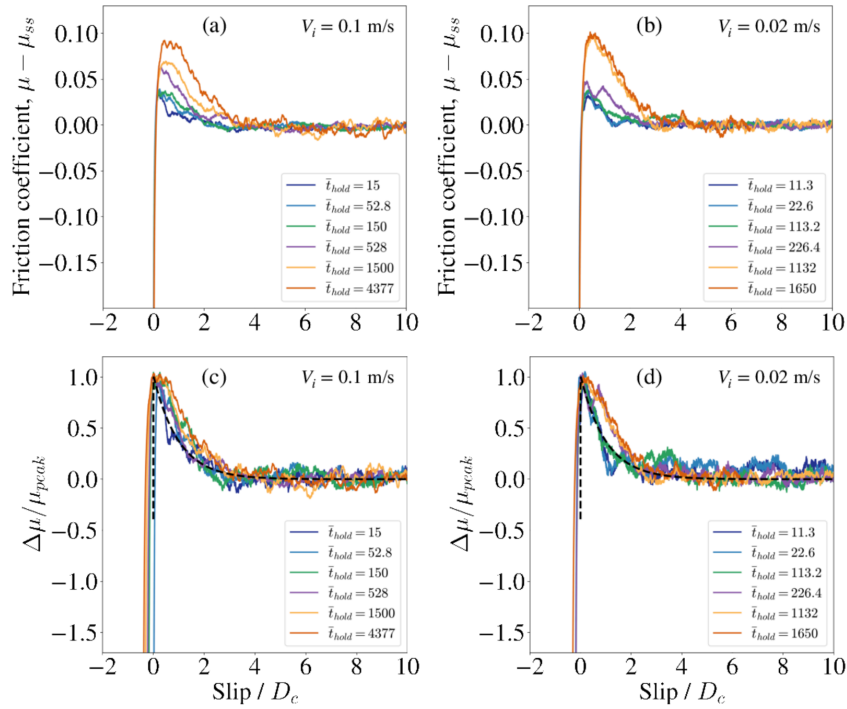


Figure 6. The variation of friction ($\mu - \mu_{ss}$) versus slip distance (Slip / D_c) during the reslide portion of slide-hold-slide simulations, for different values of normalized hold time $\bar{t}_{hold}/(D_c/V_i)$ and sliding velocities of (a) $V_i = 0.1$ m/s and (b) $V_i = 0.02$ m/s. Panels (c) and (d) show the signals in panels (a) and (b) with values normalized by the peak friction value in each simulation. All simulations are performed with stiffness $\bar{k}_d \approx 425$ at 5 MPa confining stress. The black dashed line in panels (c) and (d) show the Slip law predictions for a one order of magnitude velocity-step increase, using the RSF parameters that provide good fits to velocity steps of various sizes performed with the granular model (Ferdowsi & Rubin, 2020). The Slip law prediction is scaled to the same peak-residual scale as the granular simulation data in the panels. The lines are added to show that the slip-weakening distance D_c increases with hold duration from a minimum value that is consistent with the value appropriate for velocity steps.

584 the amount of increase in D_c in the granular model appears to be less than that observed in lab data.
 585 Sleep et al. (2000) proposed a model in which delocalization of slip within a granular layer during
 586 a hold led to an increase in the effective slip-weakening distance after a reslide, as slip gradually
 587 re-localized. If this explanation is correct, the relatively small increase in D_c that we observe could
 588 be due to the lack of obvious localization in our simulations.

589 In our SHS simulations, we have also investigated whether changing the re-sliding velocity
 590 changes either the peak friction or the approach to the future steady-state friction. Any behavior that
 591 deviates from the RSF prediction is relevant to models of earthquake nucleation, as the perimeter of
 592 an expanding nucleation zone subjects regions that have not slipped for a long time (as in a hold) to
 593 successively larger velocity jumps (Ampuero & Rubin, 2008). For this purpose, we have run reslide
 594 simulations after a hold time $\bar{t}_{hold} \sim 1650$, with the initial sliding velocity $V_i = 0.02$ m/s and reslide
 595 velocities V_r of 0.02, 0.05, 0.1, and 0.3 m/s. In a sense these are velocity-step tests, but run from
 596 a single value of state that is much larger than the steady-state value at velocity V_i . The results are
 597 shown in supplementary Fig. S2a, where friction is plotted relative to its future steady-state value.
 598 The prediction of equation (1), assuming that the change in state between the end of the hold and
 599 peak stress is either small or independent of the reslide velocity, is that the difference in $\Delta\mu_{peak}$
 600 between two reslide velocities V_2 and V_1 is equal to $b \ln(V_2/V_1)$. The inset in Fig. S2-a shows that

601 this is very nearly the case, with $\Delta\mu_{peak}$ increasing linearly with $\ln(V_r/V_i)$ with a slope of 0.0155,
 602 or 87% of the value $b = 0.0178$ measured in velocity-steps. Furthermore, scaling the $\Delta\mu$ curves by
 603 the value $[C + \ln(V_r/V_i)]$ in Fig. S2-b, with the value of $C = 5$ determined empirically (the value of
 604 $\Delta\mu_{peak}/b$ determined for $V_r = V_i$), collapses the frictional response for all the reslide velocities onto
 605 a single curve, consistent with the Slip law prediction. In other words, within the range of velocities
 606 that we have explored, changing the reslide velocity does not affect the weakening distance D_c in the
 607 granular model, consistent with the Slip law prediction, and changes the peak friction in accordance
 608 with standard RSF.

609 5 Energetics of granular slide-holds

610 Although the exact definition of an effective thermodynamic temperature for granular materials
 611 is still a matter of much debate (Ono et al., 2002; Blumenfeld & Edwards, 2009; Puckett & Daniels,
 612 2013; Bi et al., 2015; D. Richard et al., 2021), recent research results suggest that the fluctuating
 613 kinetic energy in these systems can play a role similar to the effective temperature. For this reason,
 614 the fluctuating kinetic energy in granular systems (that is, the kinetic energy determined after
 615 subtracting from the velocity vector of each grain the average velocity vector of all the grains in its
 616 immediate environment) is often referred to as the “granular temperature”, and it has proven to be an
 617 important control on the rheological behavior of these systems (Campbell, 1990; Losert et al., 2000;
 618 Kim & Kamrin, 2020). In our previous work, we found that the magnitude of the RSF direct effect
 619 parameter a in the sheared granular gouge could plausibly be explained as the ratio of the fluctuating
 620 kinetic energy to the stored potential energy in the system (Ferdowsi & Rubin, 2020), although this
 621 proposal requires further investigation. We further showed that in the quasi-static shearing regime
 622 ($V \lesssim 1$ m/s, for a normal stress of 5 MPa), the fluctuating kinetic energy becomes nearly constant,
 623 which would suggest a nearly constant magnitude of the direct effect, consistent with most laboratory
 624 rock and gouge friction experiments (Kilgore et al., 1993; Bhattacharya et al., 2015). A nearly
 625 constant value of effective granular temperature in the quasi-static regime has also been previously
 626 reported in experimental granular physics studies (Song et al., 2005; Corwin et al., 2005), although
 627 more recent studies of granular systems with different loading geometries (i.e., other than tabular
 628 gouge layers between parallel plates) shows that this behavior could be influenced by localized de-
 629 formation close to driving boundaries (Gaume et al., 2020; Kim & Kamrin, 2020; P. Richard et al.,
 630 2020).

In this work, we further examine the evolution of fluctuating kinetic energy in granular slide-
 hold simulations. The instantaneous per-grain fluctuating kinetic energy is defined in the tensorial
 form,

$$\delta E_k(t) = \frac{1}{N} \sum_{i=1}^N \delta \vec{v}_i(t) \otimes \delta \vec{v}_i(t), \quad (6)$$

631 where $\delta \vec{v}_i(t) = \vec{v}_i(t) - \vec{v}_i(z_k, t)$. In these calculations, $\vec{v}_i(z_k, t)$ is the instantaneous linear velocity
 632 field, calculated with coarse-graining of the granular model data, according to $\vec{v}_i(z_k, t) = (1/N_k) \sum_{i=1}^{N_k} \vec{v}_i(t)$,
 633 in which $v_i(t)$ is the linear velocity of the i th particle within the rectangular cuboid with dimensions
 634 ($L_x, L_y, \Delta z = 1.37 D_{mean}$), and N_k is the total number of grains within each cuboid.

635 The variation of per grain fluctuating energy δE_k with hold time for slide-holds with initial
 636 sliding velocities $V_i = 0.1$ and 0.02 m/s and three different system stiffnesses are shown in Figs. 7a
 637 and 7b, respectively. The curves appear somewhat noisy because the individual data points are
 638 snapshots and not averages over some time window. The results show that with these two initial
 639 velocities, for moderate hold times δE_k decreases log-linearly over about 4 orders of magnitude in
 640 hold time, and then plateaus at roughly 50% of its initial steady-state value. Decreasing the system
 641 stiffness delays the onset of the reduction in δE_k , presumably because this allows stresses and sliding
 642 velocities near the prior steady state to persist for longer times, but does not otherwise change the
 643 shape of the energy reduction curves. This is shown by Fig. 7c, where for both V_i we further multiply
 644 the normalized hold time \bar{t}_{hold} by $k_d^{2/3}$, resulting in the collapse of all the simulation results for each
 645 initial velocity (at this point the choice of $2/3$ for the power is strictly empirical). Plotting the change

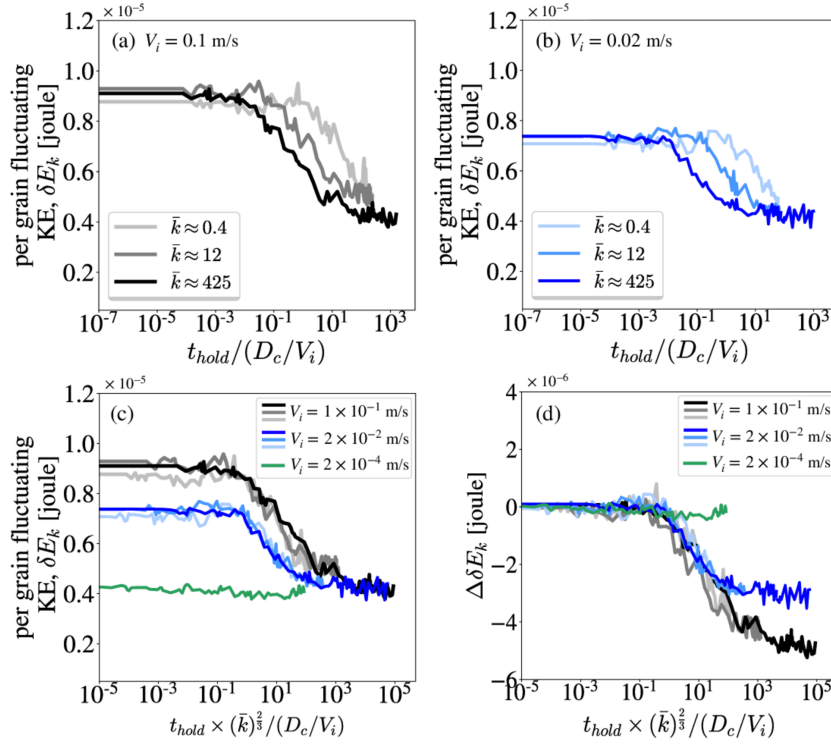


Figure 7. The variation of per grain fluctuating kinetic energy (δE_k) with hold time in slide-hold simulations performed with three system stiffnesses $\bar{k}_d \approx 425$, 12, and 0.4, at two sliding velocities of (a) $V_i = 0.1$ m/s and (b) $V_i = 0.02$ m/s. (c) The variation of δE_k with (hold time) \times (system stiffness, \bar{k}_d)² for all data shown in panels (a) and (b). (d) same as panel (c) with δE_k referenced to its initial value ($\delta E_{k,0}$) for each simulation. The green lines in panels (c) and (d) show the variation of δE_k and $\delta E_k - \delta E_{k,0}$ for simulations with sliding velocity $V_i = 2 \times 10^{-4}$ m/s and stiffness $\bar{k}_d \approx 425$. All simulations are performed at 5 MPa confining stress.

646 in δE_k from its initial steady state value further shows that the onset of the kinetic energy reduction
 647 is similar for both values of V_i (Figure 7d).

648 Figure 7c also shows that although the curves for the lower V_i have a slightly smaller δE_k at
 649 steady state ($\delta E_{k,ss}$), for all stiffnesses both V_i appear to plateau to the same value of δE_k at large
 650 hold times. This raises the question of whether there would be any reduction in δE_k during the hold
 651 for values of V_i small enough for $\delta E_{k,ss}$ to be at or below this plateau value. Ferdowsi and Rubin
 652 (2020) found that the steady-state value of δE_k decreased from about 1.7×10^{-5} J at $V = 10^{-1}$ m/s
 653 to slightly below 10^{-5} J at $V = 10^{-4}$ m/s (triangles in Figure 8b), close to the plateau value of δE_k
 654 in Figure 7c. For this reason we ran slide-hold simulations with $V = 2 \times 10^{-4}$ m/s, about the lowest
 655 value that could reach moderate values of \bar{t}_{hold} in a reasonable amount of computation time (about
 656 1.5 months). For the same reason the simulations were run only at the largest stiffness; this leads
 657 to the largest reduction in δE_k for a given \bar{t}_{hold} . We find that, indeed, δE_k for these simulations
 658 starts near the plateau value for the larger V_i in Figure 7c, and undergoes very little decay during the
 659 hold. Despite this, the stress decay, when plotted vs. dimensionless hold time, appears very similar
 660 to that for $V_i = 2 \times 10^{-2}$ and 10^{-1} m/s (supplementary Fig. S1). This result raises the possibility
 661 that the value of 0.8×10^{-5} J for δE_k represents something of a floor for this granular system, as
 662 long as stresses are large enough to drive inelastic deformation. Because of the long computation
 663 times required we have been unable to explore this under conditions of steady-state sliding, but for
 664 the largest-stiffness holds in Figure 7, the velocities at the end of the simulations were $\sim 10^{-8} - 10^{-7}$
 665 m/s for the different V_i (Fig. 8a). The variation of per grain fluctuation energy versus sliding velocity

666 during holds follows closely the trend we have observed in the steady-state simulations, although it
 667 extends that trend to much lower velocities (Fig. 8b), and this suggests the sliding velocity is likely
 668 a primary factor in controlling the fluctuating energy, whether or not the system is at quasi-steady
 669 state.

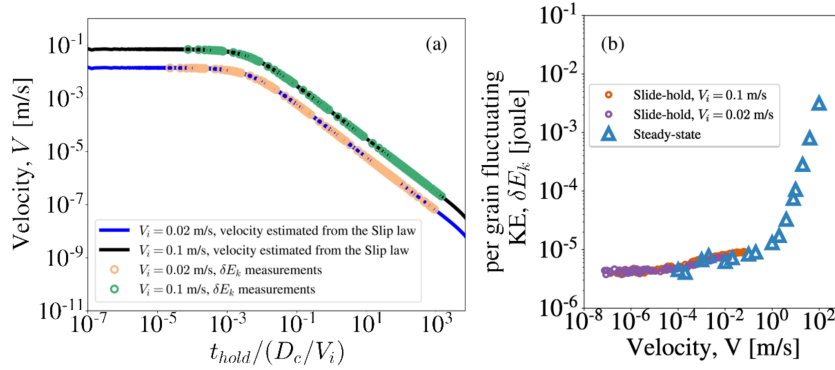


Figure 8. (a) Estimated sliding velocities during the slide-hold simulations with $\bar{k} \approx 425$ and initial sliding velocities $V_i = 0.02$ m/s and 0.1 m/s in Figure 2a (solid lines), and the times at which measurements of the per grain fluctuating kinetic energy (δE_k) were made (open circles), as functions of dimensionless hold time. Determining the slip speed directly from the simulations by taking the time-derivative of equation (4) (with $\delta I_p = 0$) results in very noisy velocity histories. Instead, we estimate the slip speed from the Slip law fit to these data. These estimated velocities equal the actual velocities whenever the simulations and the Slip law fit (solid red line in Figure 2a) have the same slope at the same value of t_{hold} . (b) The variation of per grain fluctuating kinetic energy with sliding velocity in the slide-hold simulations of panel (a) (magenta and brown circles) and in steady-state simulations reported in Ferdowsi and Rubin (2020) (blue triangles; the break in slope just below 1 m/s marks the boundary between the quasi-static and inertial regimes of flow). All simulations are performed at 5 MPa confining stress.

670 We do not yet understand what controls the nearly fixed value of the fluctuating kinetic energy
 671 at long hold times or low steady-state sliding speeds in our simulations. For as long as δE_k is nearly
 672 constant, the energy loss from grain-grain friction and inelastic collisions must be balanced by work
 673 done on the gouge by the moving upper plate (or a reduction in elastic potential energy, but this is not
 674 an option during steady sliding, and even during holds, at constant confining pressure this strikes us
 675 as a less likely source). During load-point holds this work comes from both shearing (equivalent to
 676 the potential energy loss of the attached spring) and compaction. In these high-stiffness simulations
 677 the shearing and compaction velocities are of the same order of magnitude. As both decay roughly
 678 logarithmically with time during the hold, the rate of energy loss must also decay logarithmically
 679 with time. For our default restitution coefficient ϵ of ~ 0.98 , collisions are nearly perfectly elastic
 680 and we presume that most of the energy loss is due to grain-grain friction. To explore the effect of
 681 increasing the collisional energy loss, we ran simulations with $\epsilon \sim 0.3$, for $\bar{k}_d \approx 12$. The results
 682 of these highly damped simulations are shown in Fig. 9. We find that the stress decay is nearly
 683 indistinguishable from that with the higher restitution coefficient (Figure 9a), and that while δE_k for
 684 the lower restitution coefficient is offset to lower values, the shape of the curve of fluctuating energy
 685 with hold time is not much different (Figure 9b). We conclude that within the range explored, the
 686 choice of restitution coefficient does not significantly influence the mechanical behavior of these
 687 systems at such low strain rates, consistent with previous results (MiDi, 2004; Ferdowsi & Rubin,
 688 2020).

689 If, as was proposed by Ferdowsi and Rubin (2020), the RSF direct effect parameter a is pro-
 690 portional to δE_k , then Figure 7 suggests that a might vary by a factor of ~ 2 over the duration of

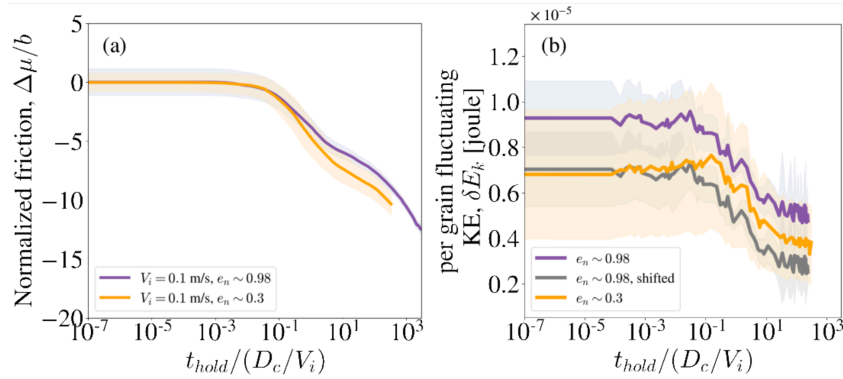


Figure 9. (a) The variation of friction coefficient, normalized by the RSF parameter b , as a function of normalized hold time, for granular slide-hold simulations with sliding velocity 10^{-1} m/s and two restitution coefficients of $\epsilon \sim 0.98$ and $\epsilon \sim 0.3$. (b) The variation of fluctuating kinetic energy with normalized hold time for the simulations in panel (a). The shaded regions indicate 2- σ standard deviations of 8 different realizations. The gray curve shows the fluctuating kinetic energy for the simulation with $\epsilon \sim 0.98$ shifted vertically.

691 the holds with the larger V_i . One could then ask if the generally good fit of the Slip law, using
 692 constant parameter values, to the decay of friction during these same holds and to laboratory data,
 693 as in Figure 2, is really supportive of the Slip law for state evolution (that is, supportive of a model
 694 in which healing does not occur in the absence of slip). For example, is it possible that the friction
 695 data could be well fit by the Aging law (that is, by a model in which healing occurs with time even
 696 in the absence of slip), given the proper velocity-dependence of a ? However, we note that for the
 697 highest-stiffness simulations in Figures 2 and 7, the continual log-linear stress decay continues to be
 698 well fit by the Slip law with constant parameter values even for dimensionless hold times larger than
 699 $\sim 10^{0.5}$, where δE_k is essentially constant. In addition, for the simulation with $V_i = 2 \times 10^{-4}$ m/s
 700 in supplementary Figure S1, δE_k is roughly constant and t_{hold} is arguably large enough to show that
 701 the friction data are more consistent with slip-dependent rather than time-dependent healing. We
 702 leave further investigation of the potential relation between measures of effective temperature and
 703 the value of a in granular simulations for future work.

704 6 Conclusions

705 In this work, we investigated the behavior of a sheared granular layer subjected to loading
 706 conditions designed to mimic laboratory slide-hold-slide experiments, for a range of sliding veloci-
 707 ties and system stiffnesses. We compared the transient frictional behavior of the model to existing
 708 rock friction data, as well as to the predictions of standard rate-state friction (RSF) constitutive
 709 equations. For the past few decades it has been common in the rock deformation and earthquake
 710 physics communities to interpret the direct rate dependence of RSF as resulting from a thermally-
 711 activated process involving the breaking of chemical bonds at contacting asperities, and to interpret
 712 state evolution as due to time-dependent plasticity (or perhaps time-dependent bond strengthening)
 713 at those asperities. We have removed this basic ingredient from our simulations, and instead ex-
 714 plored whether transient friction as observed in the laboratory could arise simply from momentum
 715 transfer in a granular layer with constant friction at grain/grain contacts. Such a granular layer might
 716 represent a natural fault gouge, or, in the laboratory context, a synthetic gouge layer, a powder that
 717 arises during slip on initially bare rock surfaces, or, owing to similarities in behavior between gran-
 718 ular systems and disordered solids (Manning & Liu, 2011; Cubuk et al., 2017), perhaps amorphous
 719 wear products on those surfaces. Simulated velocity steps in the same granular model have already
 720 shown a direct velocity-dependence and an opposing state evolution-dependence of friction, each
 721 proportional to the logarithm of the velocity jump, with magnitudes (the RSF parameters a and b) of

~0.02, not far from lab values. In addition, state evolution following the velocity jumps occurs over a slip distance that is independent of the size and sign of the velocity step, consistent with laboratory experiments and the Slip law for state evolution. A final motivation for our simulations is that while the RSF equations are largely empirical, the granular model is physics-based, and its output allows us to investigate and perhaps understand why it behaves as it does.

The behavior of the granular flow model in slide-hold simulations appears to closely resemble laboratory experiments in two important respects. First, the continual stress decay during the hold is reasonably well modeled by the Slip version of the RSF equations, using parameter values determined independently from velocity step tests on the identical system. This is consistent with lab data, as is the result that for both the granular simulations and lab data, the Aging version of the RSF equations predicts too little stress decay. This is because it predicts too much healing, i.e. state evolution, which for the Aging law progresses with time rather than slip (Bhattacharya et al., 2017, 2021). Under standard RSF, with no intrinsic velocity scale, the stress decay as a function of normalized hold time $t_{hold}/(D_c/V_i)$ must be independent of the initial sliding velocity V_i . This is approximately the case for our stiffest simulations ($\bar{k} \sim 425$), but larger differences arise for the stiffnesses more appropriate for lab experiments ($\bar{k} \sim 12$ and 0.4), where the prediction of the Slip law falls roughly between the simulation results. There is not much lab data investigating this question. The experiments of (Marone & Saffer, 2015) on simulated gouge show a modest dependence on V_i , when plotted vs. normalized hold time, but the sign of that dependence seems to be opposite from our granular simulations. The experiments of Carpenter et al. (2016), however, do not show this dependence. The source of the V_i -dependence in the granular simulations, and whether it might be related to the variation of δE_k for $10^{-4} \lesssim V \lesssim 10^{-1}$ m/s in Figure 8b, is unknown.

Second, in both the granular simulations and laboratory experiments, the fault layer undergoes compaction roughly linearly with log time. Even the rates are roughly comparable, at $\sim 0.05D_c$ per decade of hold time in Figure 4. Log-time compaction is consistent with standard interpretations of the time-dependent Aging law for state evolution (compaction being a proxy for growth of true contact area), even though in both the granular simulations and lab experiments the stress decay is consistent with the Slip law and not the Aging law. As with the large velocity-step decreases described by Ferdowsi and Rubin (2020), this suggests a decoupling between state evolution and changes in fault or gouge thickness, in both the lab and the granular simulations, that seems inconsistent with traditional interpretations of RSF (Sleep, 2006, e.g.).

The reslide portions of our granular slide-hold-slide simulations share with laboratory experiments the result that, for sufficiently long holds, the peak friction upon resliding (“frictional healing”, $\Delta\mu_{peak}$) increases nearly linearly with the logarithm of hold time (J. H. Dieterich, 1972; Marone et al., 1990). For our maximum stiffness and larger lab-like stiffness ($\bar{k} \approx 12$), the long-time healing rate $d\Delta\mu_{peak}/d\ln(\bar{t}_{hold})$ is very close to the RSF evolution-effect parameter b , as predicted by the Aging law for all stiffnesses, but for our smaller lab-like stiffness ($\bar{k} \approx 0.4$) it is only half that value. The range of slopes we find is close to the range $\sim 0.3 - 0.7b$ seen in a study where the value of b was determined independently from velocity-step tests (Ikari et al., 2016; Carpenter et al., 2016). However, unlike the lab data of Beeler et al. (1994), we find this slope to be dependent upon the stiffness of the testing apparatus, by a factor of 2. System stiffness is potentially important because it controls the amount of interfacial slip during the load-point hold; for our longest hold durations this slip is $\sim D_c$ for our larger lab-like stiffness, and $\sim 10D_c$ for our smaller. However, the effect of stiffness on healing rates in our simulations and in lab data seems to be at most rather modest.

There also appears to be no influence of the initial sliding velocity V_i on the rate of frictional healing at long times in our SHS simulations. In this respect they are similar to the laboratory experiments of Carpenter et al. (2016), but not Marone and Saffer (2015), both conducted in the range $V_i = 1 - 100 \mu\text{m/s}$, somewhat below to far below the velocities we could achieve.

To summarize, the granular model mimics laboratory slide-hold experiments in that the stress decay during the hold is well approximated by the Slip law for state evolution, using parameter values determined from velocity steps on the same sample. In addition, both the granular simulations and laboratory experiments undergo roughly log-time compaction at comparable rates, when those

774 rates are normalized by the appropriate value of D_c . For slide-hold-slide protocols, the granular
 775 model mimics laboratory experiments in that the rate of healing at sufficiently long hold times is
 776 roughly linear with log time, with a slope that is near to that observed in the lab (a modest fraction
 777 of b). Thus, despite several shortcomings, including the use of spherical grains with a geologi-
 778 cally narrow size distribution, and a range of sliding velocities that, due to computational expense,
 779 are very high by lab standards, it can still be argued that the granular model does a better job of
 780 matching laboratory experiments than existing, and empirical, rate-state friction equations. Unlike
 781 the comparison of velocity-step simulations to lab experiments emphasized by Ferdowsi and Rubin
 782 (2020), for the SHS protocols there are clearly some failures as well as successes of the granular
 783 model. It is entirely possible that some of these failures are due to time-dependent contact-scale
 784 processes in lab experiments that we specifically excluded from our simulations.

785 Researchers in the fields of granular physics and granular rheology have previously found that
 786 the fluctuating kinetic energy, δE_k , sometimes referred to as the “granular temperature”, in part
 787 controls the rheology of these materials in steady-state and some transient regimes (Kim & Kamrin,
 788 2020; Gaume et al., 2020; Campbell, 1990). In our previous study, we found that although δE_k
 789 varied with confining pressure, the ratio of δE_k to elastic strain energy within the gouge varied only
 790 slightly with pressure and steady-state sliding speed, and was close to the (also nearly constant) value
 791 of the direct velocity effect parameter a of the granular layer (Ferdowsi & Rubin, 2020). In that
 792 paper we evaluated the variation in fluctuating kinetic energy at steady-state shear velocities as low
 793 as 10^{-4} m/s. In the slide-hold simulations reported here, we find that δE_k becomes even more nearly
 794 constant down to transient sliding velocities below 10^{-7} m/s. We also find here that changing the
 795 damping (energy loss) for grain-grain interactions does not substantially alter the variation of δE_k ,
 796 or the stress decay during holds, for the range of parameters explored. Further understanding what
 797 controls the changes in fluctuating kinetic energy, its near-constant value in the quasi-static limit,
 798 and its relation to the direct effect parameter a , may guide future studies of the proper formulations
 799 of rate-and-state friction laws for describing the transient frictional response of granular layers, and
 800 for connecting the RSF framework to more physics-based models.

801 Additional future research may explore recent definitions of state variable for amorphous ma-
 802 terials (e.g., D. Richard et al. (2021)) in the context of elastoviscoplastic rheology for soft glassy
 803 materials (e.g., Fielding (2020)). These works may also address the applications of some of the
 804 latest developments in constitutive modeling of complex fluids with potentially similar (but as-yet
 805 unexplored in the context of rock and sediment friction) rate-dependent rheological response and
 806 hysteresis to rate- and state-dependent behavior of Earth materials. Also, our study here has been
 807 focused on the stress relaxation and healing behavior of a sheared granular layer that shows velocity-
 808 strengthening frictional behavior. It has been recently observed that, even without implementing
 809 any sophisticated or time-dependent grain-contact scale processes in granular simulations, granular
 810 models that use certain grain shapes (Salerno et al., 2018), or grain-grain contact potentials/laws in
 811 certain regions of normal pressure and grain stiffness (such as the Hookean contact law, in the grain
 812 strain range smaller than 10^{-3} (Kim & Kamrin, 2020; DeGiuli & Wyart, 2017)) show velocity-
 813 weakening friction in the dense quasi-static flow regime. Exploring the transient rheology of such
 814 velocity-weakening systems in velocity-step and slide-hold-slide protocols, may provide more in-
 815 sights into the physics of granular rate-state behavior, and additional opportunities for comparing
 816 the behavior of the granular model to lab data when both are in the velocity-weakening regime of
 817 friction.

818 **Acknowledgments**

819 BF acknowledges support from the Department of Geosciences, Princeton University, in form of a
 820 Harry H. Hess postdoctoral fellowship. Research was sponsored by the US National Science Foun-
 821 dation (NSF) awards EAR-1547286 and EAR-1946434, by the US Geological Survey (USGS),
 822 Department of the Interior, awards G19AP00048 and G20AP00112, and by the US Army Research
 823 Office (ARO) award W911NF-20-1-0154, all of the awards to AMR. The authors thank Pathikrit
 824 Bhattacharya, Terry E. Tullis, Nicholas M. Beeler, and Keishi Okazaki, for their permission to use
 825 the data shown in Figure 2d of this manuscript. Parallel programs were run on computers provided

826 by the Princeton Institute for Computational Science and Engineering (PICSciE). The 3-D visual-
 827 izations of the model were performed using the open-source visualization software “The Persistence
 828 of Vision Raytracer” POV-Ray (<http://www.povray.org>). Most of the data analysis were carried out
 829 using the open-source Python library, NumPy (<https://numpy.org>). The 2-D plots were made with
 830 the Python library Matplotlib (www.matplotlib.org). The computer codes for LAMMPS simula-
 831 tions of this paper with the information about the version of LAMMPS used for the simulations,
 832 are available on the Dryad digital repository at <https://doi.org/10.5061/dryad.2z34tmphk>. The views
 833 and conclusions contained in this document are those of the authors and should not be interpreted as
 834 necessarily representing the official policies, either expressed or implied, of the U.S. Government.

835 References

- 836 Abe, S., Dieterich, J. H., Mora, P., & Place, D. (2002). Simulation of the influence of rate-and
 837 state-dependent friction on the macroscopic behavior of complex fault zones with the lattice
 838 solid model. *pure and applied geophysics*, *159*(9), 1967–1983.
- 839 Ampuero, J.-P., & Rubin, A. M. (2008). Earthquake nucleation on rate and state faults—aging and
 840 slip laws. *Journal of Geophysical Research: Solid Earth*, *113*(B1).
- 841 Baumberger, T., Berthoud, P., & Caroli, C. (1999). Physical analysis of the state-and rate-dependent
 842 friction law. ii. dynamic friction. *Physical Review B*, *60*(6), 3928.
- 843 Baumberger, T., & Caroli, C. (2006). Solid friction from stick–slip down to pinning and aging.
 844 *Advances in Physics*, *55*(3-4), 279–348.
- 845 Beeler, N., Tullis, T., Blanpied, M., & Weeks, J. (1996). Frictional behavior of large displacement
 846 experimental faults. *Journal of Geophysical Research: Solid Earth*, *101*(B4), 8697–8715.
- 847 Beeler, N., Tullis, T., & Weeks, J. (1994). The roles of time and displacement in the evolution effect
 848 in rock friction. *Geophysical Research Letters*, *21*(18), 1987–1990.
- 849 Berthoud, P., Baumberger, T., G’sell, C., & Hiver, J.-M. (1999). Physical analysis of the state-and
 850 rate-dependent friction law: Static friction. *Physical review B*, *59*(22), 14313.
- 851 Bhattacharya, P., Rubin, A. M., Bayart, E., Savage, H. M., & Marone, C. (2015). Critical evaluation
 852 of state evolution laws in rate and state friction: Fitting large velocity steps in simulated
 853 fault gouge with time-, slip-, and stress-dependent constitutive laws. *Journal of Geophysical
 854 Research: Solid Earth*, *120*(9), 6365–6385.
- 855 Bhattacharya, P., Rubin, A. M., & Beeler, N. M. (2017). Does fault strengthening in laboratory rock
 856 friction experiments really depend primarily upon time and not slip? *Journal of Geophysical
 857 Research: Solid Earth*.
- 858 Bhattacharya, P., Rubin, A. M., Tullis, T. E., Beeler, N. M., & Okazaki, K. (2021). The evolution of
 859 rock friction is more sensitive to slip than elapsed time, even at near-zero slip rates. *Earth and
 860 Space Science Open Archive*. Retrieved from [https://doi.org/10.1002/essoar](https://doi.org/10.1002/essoar.10507717.1)
 861 .10507717.1 doi: 10.1002/essoar.10507717.1
- 862 Bi, D., Henkes, S., Daniels, K. E., & Chakraborty, B. (2015). The statistical physics of athermal
 863 materials. *Annu. Rev. Condens. Matter Phys.*, *6*(1), 63–83.
- 864 Blanpied, M., Marone, C., Lockner, D., Byerlee, J., & King, D. (1998). Quantitative measure of the
 865 variation in fault rheology due to fluid-rock interactions. *Journal of Geophysical Research:
 866 Solid Earth*, *103*(B5), 9691–9712.
- 867 Blumenfeld, R., & Edwards, S. F. (2009). On granular stress statistics: Compactivity, angoricity,
 868 and some open issues. *The Journal of Physical Chemistry B*, *113*(12), 3981–3987.
- 869 Brilliantov, N. V., Spahn, F., Hertzsch, J.-M., & Pöschel, T. (1996). Model for collisions in granular
 870 gases. *Physical review E*, *53*(5), 5382.
- 871 Campbell, C. S. (1990). Rapid granular flows. *Annual Review of Fluid Mechanics*, *22*(1), 57–90.
- 872 Carpenter, B. M., Ikari, M. J., & Marone, C. (2016). Laboratory observations of time-dependent
 873 frictional strengthening and stress relaxation in natural and synthetic fault gouges. *Journal of
 874 Geophysical Research: Solid Earth*, *121*(2), 1183–1201.
- 875 Chen, J., & Spiers, C. J. (2016). Rate and state frictional and healing behavior of carbonate fault
 876 gouge explained using microphysical model. *Journal of Geophysical Research: Solid Earth*,
 877 *121*(12), 8642–8665.

- 878 Chen, J., van den Ende, M. P., & Niemeijer, A. R. (2020). Microphysical model predictions of
879 fault restrengthening under room-humidity and hydrothermal conditions: From logarithmic to
880 power-law healing. *Journal of Geophysical Research: Solid Earth*, *125*(4), e2019JB018567.
- 881 Corwin, E. I., Jaeger, H. M., & Nagel, S. R. (2005). Structural signature of jamming in granular
882 media. *Nature*, *435*(7045), 1075.
- 883 Cubuk, E. D., Ivancic, R., Schoenholz, S. S., Strickland, D., Basu, A., Davidson, Z., ... others
884 (2017). Structure-property relationships from universal signatures of plasticity in disordered
885 solids. *Science*, *358*(6366), 1033–1037.
- 886 da Cruz, F., Emam, S., Prochnow, M., Roux, J.-N., & Chevoir, F. (2005). Rheophysics of dense gran-
887 ular materials: Discrete simulation of plane shear flows. *Physical Review E*, *72*(2), 021309.
- 888 DeGiuli, E., & Wyart, M. (2017). Friction law and hysteresis in granular materials. *Proceedings of
889 the National Academy of Sciences*, *114*(35), 9284–9289.
- 890 Dieterich, J. (1994). A constitutive law for rate of earthquake production and its application to
891 earthquake clustering. *Journal of Geophysical Research: Solid Earth*, *99*(B2), 2601–2618.
- 892 Dieterich, J. H. (1972). Time-dependent friction in rocks. *Journal of Geophysical Research*, *77*(20),
893 3690–3697.
- 894 Dieterich, J. H. (1978). Time-dependent friction and the mechanics of stick-slip. In *Rock friction
895 and earthquake prediction* (pp. 790–806). Springer.
- 896 Dieterich, J. H. (1979). Modeling of rock friction: 1. experimental results and constitutive equations.
897 *Journal of Geophysical Research: Solid Earth*, *84*(B5), 2161–2168.
- 898 Dieterich, J. H. (1992). Earthquake nucleation on faults with rate-and state-dependent strength.
899 *Tectonophysics*, *211*(1-4), 115–134.
- 900 Dieterich, J. H., & Kilgore, B. (1996). Implications of fault constitutive properties for earthquake
901 prediction. *Proceedings of the National Academy of Sciences*, *93*(9), 3787–3794.
- 902 Dieterich, J. H., & Kilgore, B. D. (1994). Direct observation of frictional contacts: New insights for
903 state-dependent properties. *Pure and Applied Geophysics*, *143*(1), 283–302.
- 904 Dieterich, J. H., et al. (1981). Constitutive properties of faults with simulated gouge. *Mechanical
905 Behavior of*.
- 906 Ferdowsi, B., & Rubin, A. M. (2020). A granular-physics-based view of fault friction experiments.
907 *Journal of Geophysical Research: Solid Earth*, e2019JB019016.
- 908 Fielding, S. M. (2020). Elastoviscoplastic rheology and aging in a simplified soft glassy constitutive
909 model. *Journal of Rheology*, *64*(3), 723–738.
- 910 Forterre, Y., & Pouliquen, O. (2008). Flows of dense granular media. *Annu. Rev. Fluid Mech.*, *40*,
911 1–24.
- 912 Frye, K. M., & Marone, C. (2002). Effect of humidity on granular friction at room temperature.
913 *Journal of Geophysical Research: Solid Earth*, *107*(B11), ETG–11.
- 914 Gaume, J., Chambon, G., & Naaim, M. (2011). Quasistatic to inertial transition in granular materials
915 and the role of fluctuations. *Physical Review E*, *84*(5), 051304.
- 916 Gaume, J., Chambon, G., & Naaim, M. (2020). Microscopic origin of nonlocal rheology in dense
917 granular materials. *Physical Review Letters*, *125*(18), 188001.
- 918 Handwerker, A. L., Rempel, A. W., Skarbek, R. M., Roering, J. J., & Hilley, G. E. (2016). Rate-
919 weakening friction characterizes both slow sliding and catastrophic failure of landslides. *Pro-
920 ceedings of the National Academy of Sciences*, *113*(37), 10281–10286.
- 921 Hatano, T. (2009). Scaling of the critical slip distance in granular layers. *Geophysical Research
922 Letters*, *36*(18).
- 923 Ikari, M. J., Carpenter, B. M., & Marone, C. (2016). A microphysical interpretation of rate-and
924 state-dependent friction for fault gouge. *Geochemistry, Geophysics, Geosystems*, *17*(5), 1660–
925 1677.
- 926 Johnson, K. L. (1987). *Contact mechanics*. Cambridge University Press.
- 927 Kato, N., & Tullis, T. E. (2001). A composite rate-and state-dependent law for rock friction.
928 *Geophysical research letters*, *28*(6), 1103–1106.
- 929 Kilgore, B. D., Blanpied, M. L., & Dieterich, J. H. (1993). Velocity dependent friction of granite
930 over a wide range of conditions. *Geophysical Research Letters*, *20*(10), 903–906.
- 931 Kim, S., & Kamrin, K. (2020, Aug). Power-law scaling in granular rheology across flow geomet-
932 ries. *Phys. Rev. Lett.*, *125*, 088002. Retrieved from <https://link.aps.org/doi/>

- 10.1103/PhysRevLett.125.088002 doi: 10.1103/PhysRevLett.125.088002
- 933 Landau, L. D., & Lifshitz, E. M. (1959). Theory of elasticity.
- 934 Li, Q., Tullis, T. E., Goldsby, D., & Carpick, R. W. (2011). Frictional ageing from interfacial
935 bonding and the origins of rate and state friction. *Nature*, *480*(7376), 233.
- 936 Liu, Y., & Szlufarska, I. (2012). Chemical origins of frictional aging. *Physical review letters*,
937 *109*(18), 186102.
- 938 Losert, W., Bocquet, L., Lubensky, T., & Gollub, J. P. (2000). Particle dynamics in sheared granular
939 matter. *Physical review letters*, *85*(7), 1428.
- 940 Manning, M. L., & Liu, A. J. (2011). Vibrational modes identify soft spots in a sheared disordered
941 packing. *Physical Review Letters*, *107*(10), 108302.
- 942 Marone, C. (1998). Laboratory-derived friction laws and their application to seismic faulting.
943 *Annual Review of Earth and Planetary Sciences*, *26*(1), 643–696.
- 944 Marone, C., Raleigh, C. B., & Scholz, C. (1990). Frictional behavior and constitutive modeling of
945 simulated fault gouge. *Journal of Geophysical Research: Solid Earth*, *95*(B5), 7007–7025.
- 946 Marone, C., & Saffer, D. (2015). The mechanics of frictional healing and slip instability during the
947 seismic cycle. In G. Schubert (Ed.), *Treatise on geophysics (second edition)* (Second Edition
948 ed., p. 111 - 138). Oxford: Elsevier. Retrieved from [http://www.sciencedirect](http://www.sciencedirect.com/science/article/pii/B9780444538024000920)
949 [.com/science/article/pii/B9780444538024000920](http://www.sciencedirect.com/science/article/pii/B9780444538024000920) doi: [https://doi.org/10](https://doi.org/10.1016/B978-0-444-53802-4.00092-0)
950 [.1016/B978-0-444-53802-4.00092-0](https://doi.org/10.1016/B978-0-444-53802-4.00092-0)
- 951 McCarthy, C., Savage, H., & Nettles, M. (2017). Temperature dependence of ice-on-rock friction at
952 realistic glacier conditions. *Philosophical Transactions of the Royal Society A: Mathematical,*
953 *Physical and Engineering Sciences*, *375*(2086), 20150348.
- 954 MiDi, G. (2004). On dense granular flows. *European Physical Journal E–Soft Matter*, *14*(4).
- 955 Mindlin, R. D. (1949). Compliance of elastic bodies in contact. *J. Appl. Mech., ASME*, *16*, 259–268.
- 956 Morgan, J. K. (2004). Particle dynamics simulations of rate-and state-dependent frictional sliding of
957 granular fault gouge. In *Computational earthquake science part i* (pp. 1877–1891). Springer.
- 958 Nagata, K., Nakatani, M., & Yoshida, S. (2012). A revised rate-and state-dependent friction law ob-
959 tained by constraining constitutive and evolution laws separately with laboratory data. *Journal*
960 *of Geophysical Research: Solid Earth*, *117*(B2).
- 961 Nakatani, M. (1998). A new mechanism of slip weakening and strength recovery of friction asso-
962 ciated with the mechanical consolidation of gouge. *Journal of Geophysical Research: Solid*
963 *Earth*, *103*(B11), 27239–27256.
- 964 Nakatani, M. (2001). Conceptual and physical clarification of rate and state friction: Frictional
965 sliding as a thermally activated rheology. *Journal of Geophysical Research: Solid Earth*,
966 *106*(B7), 13347–13380.
- 967 Ono, I. K., O’Hern, C. S., Durian, D. J., Langer, S. A., Liu, A. J., & Nagel, S. R. (2002). Effective
968 temperatures of a driven system near jamming. *Physical review letters*, *89*(9), 095703.
- 969 Plimpton, S. (1995). Fast parallel algorithms for short-range molecular dynamics. *Journal of*
970 *computational physics*, *117*(1), 1–19.
- 971 Puckett, J. G., & Daniels, K. E. (2013). Equilibrating temperaturelike variables in jammed granular
972 subsystems. *Physical Review Letters*, *110*(5), 058001.
- 973 Richard, D., Kapteijns, G., Giannini, J. A., Manning, M. L., & Lerner, E. (2021, Jan). Sim-
974 ple and broadly applicable definition of shear transformation zones. *Phys. Rev. Lett.*, *126*,
975 015501. Retrieved from [https://link.aps.org/doi/10.1103/PhysRevLett](https://link.aps.org/doi/10.1103/PhysRevLett.126.015501)
976 [.126.015501](https://link.aps.org/doi/10.1103/PhysRevLett.126.015501) doi: 10.1103/PhysRevLett.126.015501
- 977 Richard, P., Artoni, R., Valance, A., & Delannay, R. (2020). Influence of lateral confinement on
978 granular flows: comparison between shear-driven and gravity-driven flows. *Granular Matter*,
979 *22*(4), 1–13.
- 980 Ruina, A. (1983). Slip instability and state variable friction laws. *Journal of Geophysical Research:*
981 *Solid Earth (1978–2012)*, *88*(B12), 10359–10370.
- 982 Salerno, K. M., Bolintineanu, D. S., Grest, G. S., Lechman, J. B., Plimpton, S. J., Srivastava, I.,
983 & Silbert, L. E. (2018). Effect of shape and friction on the packing and flow of granular
984 materials. *Physical Review E*, *98*(5), 050901.
- 985 Silbert, L. E., Ertaş, D., Grest, G. S., Halsey, T. C., Levine, D., & Plimpton, S. J. (2001). Gran-
986 ular flow down an inclined plane: Bagnold scaling and rheology. *Physical Review E*, *64*(5),
987

051302.

988
989
990
991
992
993
994
995
996
997
998
999
1000
1001
1002
1003
1004
1005
1006
1007
1008
1009
1010
1011
1012
1013
1014

- Sleep, N. H. (1995). Ductile creep, compaction, and rate and state dependent friction within major fault zones. *Journal of Geophysical Research: Solid Earth*, *100*(B7), 13065–13080.
- Sleep, N. H. (1997). Application of a unified rate and state friction theory to the mechanics of fault zones with strain localization. *Journal of Geophysical Research: Solid Earth*, *102*(B2), 2875–2895.
- Sleep, N. H. (2006). Real contacts and evolution laws for rate and state friction. *Geochemistry, Geophysics, Geosystems*, *7*(8).
- Sleep, N. H., Richardson, E., & Marone, C. (2000). Physics of friction and strain rate localization in synthetic fault gouge. *Journal of Geophysical Research: Solid Earth*, *105*(B11), 25875–25890.
- Song, C., Wang, P., & Makse, H. A. (2005). Experimental measurement of an effective temperature for jammed granular materials. *Proceedings of the National Academy of Sciences*, *102*(7), 2299–2304.
- Thom, C., Carpick, R., & Goldsby, D. (2018). Constraints on the physical mechanism of frictional aging from nanoindentation. *Geophysical Research Letters*, *45*(24), 13–306.
- Tian, K., Goldsby, D. L., & Carpick, R. W. (2018). Rate and state friction relation for nanoscale contacts: Thermally activated prandtl-tomlinson model with chemical aging. *Physical Review Letters*, *120*(18), 186101.
- Tian, K., Gosvami, N. N., Goldsby, D. L., Liu, Y., Szlufarska, I., & Carpick, R. W. (2017). Load and time dependence of interfacial chemical bond-induced friction at the nanoscale. *Physical review letters*, *118*(7), 076103.
- Viesca, R. C. (2016). Self-similar slip instability on interfaces with rate-and state-dependent friction. *Proceedings of the Royal Society A: Mathematical, Physical and Engineering Sciences*, *472*(2192), 20160254.
- Zhang, H., & Makse, H. (2005). Jamming transition in emulsions and granular materials. *Physical Review E*, *72*(1), 011301.